Tubulin polyglutamylation is a general traffic-control mechanism in hippocampal neurons

Satish Bodakuntla, Anne Schnitzler, Cristopher Villablanca, Christian González-Billault, Ivan Bieche, Carsten Janke, Maria M. Magiera

Tubulin polyglutamylation is a general traffic control mechanism in hippocampal neurons

Satish Bodakuntla[1,2], Anne Schnitzler[3], Cristopher Villablanca[4,5], Christian Gonzalez-Billault[4,5], Ivan Bieche[3,6], Carsten Janke[1,2]*, Maria M. Magiera[1,2]*

[1]Institut Curie, PSL Research University, CNRS UMR3348, F-91405 Orsay, France

[2]Université Paris Sud, Université Paris-Saclay, CNRS UMR3348, F-91405 Orsay, France

[3]Institut Curie, PSL Research University, Department of Genetics, F-75005, Paris, France

[4]Center for Geroscience, Brain Health and Metabolism (GERO), Santiago, Chile

[5]Department of Biology, Faculty of Sciences, University of Chile, Santiago, Chile

[6]Université Paris Descartes, Sorbonne Paris Cité, F-75005, Paris, France

Running title: Tubulin glutamylation controls axonal traffic

*corresponding authors:

Maria M. Magiera
Carsten Janke
Institut Curie, Centre Universitaire, Bâtiment 110, F-91405 Orsay Cedex, France
Emails: Maria.Magiera@curie.fr, Carsten.Janke@curie.fr
Telephone: +33 1 69863127

Abstract

Neurons are highly complex cells that heavily rely on intracellular transport to distribute a range of functionally essential cargoes within the cell. Posttranslational modifications of tubulin are emerging mechanisms to regulate microtubule functions, but their impact on neuronal transport is only marginally understood. Here we have systematically studied the impact of posttranslational polyglutamylation on axonal transport. In cultured hippocampal neurons, deletion of a single deglutamylase, CCP1, is sufficient to induce abnormal accumulation of polyglutamylation, i.e. hyperglutamylation. We next investigated how hyperglutamylation affects axonal transport of a range of functionally different neuronal cargoes: mitochondria, lysosomes, LAMP1 endosomes and BDNF vesicles. Strikingly, we found a reduced motility for all these cargoes, suggesting that polyglutamylation could act as a central regulator of cargo transport in neurons. This, together with the recent discovery that hyperglutamylation induces neurodegeneration, makes it likely that perturbed neuronal traffic could be one of the central molecular causes underlying this novel type of degeneration.

INTRODUCTION

Neurons are the basic structural and functional units of the brain. Insights on how they function as individual cells in a complex neuronal network is instrumental for the bottom-up understanding of brain functions. Our brain contains a vast variety of different types of neurons (Zeng and Sanes, 2017). Some of them are very complex, with long axons (Cavanagh, 1984) and dendritic trees that can be highly ramified (DeFelipe, 2013). Establishment and maintenance of these complex cell morphologies, which is fundamental for the normal function of the brain (Bentley and Banker, 2016), relies to a large extent on the microtubule cytoskeleton (Conde and Caceres, 2009). In fully developed, i.e. differentiated neurons, one of the key functions of microtubules is intracellular transport (Nirschl et al., 2017), which ensures the delivery of a large variety of functionally different cargoes, such as organelles (mitochondria, lysosomes, and endosomes), proteins or mRNAs to specific target sites inside axons or dendrites (Maday et al., 2014). A key question is thus how transport of those different cargoes is temporally and spatially controlled in order to meet the ever-changing requirements of different neuronal compartments, for instance synapses, which need to be replenished in receptors for their activity (Choquet and Triller, 2013).

There are several examples demonstrating that different cargos can be independently regulated in neurons: During neuronal differentiation, mitochondria motility has been shown to progressively decrease, while the transport of late (Rab7-postive) endosomes remained unchanged (Zhou et al., 2016). Even more strikingly, axonal transport of brain-derived neurotrophic factor (BDNF) vesicles was increased while mitochondria motility decreased in differentiating neurons (Moutaux et al., 2018). The independent regulation of mitochondria and BDNF vesicle transport has been further confirmed in cultured neurons from a Huntington's disease mouse model, where BDNF-vesicle transport was reduced, while at the same time mitochondria showed enhanced motility and fragmentation (Virlogeux et al., 2018). These examples illustrate that transport of different axonal cargoes can be independently regulated, however underlying regulatory mechanisms are not fully understood.

An emerging hypothesis proposes that posttranslational modifications (PTMs; Janke, 2014) of microtubule tracks act as "traffic signs", which are recognized by cargo transporters to control their movements, thus guiding them to their final destinations. A first indication that this could indeed be the case was recently described in dendrites, where anterograde and

retrograde transport events take place on microtubules of different polarity, labelled by two distinct PTMs, acetylation and tyrosination (Tas et al., 2017). At this point it remains unclear if the PTMs are mere markers of those two microtubule populations, or if they participate in guiding the cargo transporters.

A PTM that has attracted attention as potential active regulator of neuronal traffic is polyglutamylation. This PTM generates branch chains of glutamate residues on both, α- and β-tubulin (Alexander et al., 1991; Eddé et al., 1990; Rüdiger et al., 1992), thus generating a variety of distinct polyglutamylation patterns, which in turn could destine microtubules to unique functions, e.g. to transport specific cargoes. Initial observations had already shown that altered polyglutamylation could control the delivery of synaptic cargoes (Maas et al., 2009), and we and others have recently demonstrated that abnormally increased polyglutamylation leads to defects in axonal mitochondria transport (Gilmore-Hall et al., 2019; Magiera et al., 2018).

Until now, however, it has remained unclear if polyglutamylation is a general traffic regulator in neurons, or if this PTM rather controls only selected cargoes. Moreover, polyglutamylation levels and patterns are controlled by a variety of enzymes. Polyglutamylases, which are members of the Tubulin Tyrosine Ligase Like (TTLL) family (Janke et al., 2005; van Dijk et al., 2007), and deglutamylases, which belong to the Cytosolic Carboxypeptidase (CCP) family (Rogowski et al., 2010; Tort et al., 2014), show different enzymatic characteristics, and are differentially expressed in different cell types (Ikegami et al., 2006; Kalinina et al., 2007). Their selective expression and/or activation in cells could thus contribute to the generation of characteristic polyglutamylation patterns on microtubule tracks, which in turn could provide specific signatures that are recognized by only a restricted set of readers. Here we test the impact of two different deglutamylases, CCP1 and CCP6, on polyglutamylation levels in cultured hippocampal neurons, and how excessive polyglutamylation, or hyperglutamylation, affects axonal trafficking of functionally diverse cargoes.

RESULTS

Loss of *Ccp1* alone is sufficient to induce tubulin hyperglutamylation in cultured hippocampal neurons

We have previously shown that lack of the deglutamylase *Ccp1* leads to massive and lasting accumulation of hyperglutamylated tubulin in the cerebellum and the olfactory bulb. In contrast, other brain regions, such as the cerebral cortex and hippocampus, showed nearly normal levels of polyglutamylation in adult *ccp1*$^{-/-}$ mice (Magiera et al., 2018; Rogowski et al., 2010). Removal of a second deglutamylase, CCP6, resulted in a strong hyperglutamylation of all brain regions including cerebral cortex and hippocampus, indicating that these two enzymes play complementary roles in controlling polyglutamylation patterns in those brain regions. *Ccp1*$^{-/-}$*ccp6*$^{-/-}$ mice showed neurodegeneration of pyramidal neurons in the cerebral cortex, which was observed in neither *ccp1*$^{-/-}$ nor *ccp6*$^{-/-}$ mice, and thus likely to be a direct result of hyperglutamylation (Magiera et al., 2018).

To investigate the cellular mechanisms affected by the absence of these two deglutamylases, we used cultured primary hippocampal neurons (Kaech and Banker, 2006) in which the knockout of both, *Ccp1* and *Ccp6* was induced by cre-mediated recombination, leading to a massive increase in polyglutamylation in these neurons (Bodakuntla et al., 2019a). At the same time, however, we had observed that polyglutamylation is also increased in hippocampi of young *ccp1*$^{-/-}$ mice, but in contrast to *ccp1*$^{-/-}$*ccp6*$^{-/-}$ mice, did not persist into adulthood (Magiera et al., 2018). As this suggested that loss of *Ccp1* alone might be sufficient to induce tubulin hyperglutamylation in young hippocampal neurons, we directly compared induced *ccp1*$^{-/-}$*ccp6*$^{-/-}$ with *ccp1*$^{-/-}$ neurons. As previously shown (Bodakuntla et al., 2019a; Magiera et al., 2018), expression of cre-recombinase in *Ccp1*$^{flox/flox}$*Ccp6*$^{flox/flox}$ neurons resulted in hyperglutamylation of tubulin. Strikingly, a direct comparison on the same immunoblot showed that *ccp1*$^{-/-}$ neurons have a similar, or even slightly higher level of hyperglutamylation as compared to induced *ccp1*$^{-/-}$*ccp6*$^{-/-}$ neurons at DIV4 (4 days *in vitro*; Fig. 1A). Two tubulin PTMs that had previously been linked to axonal transport, acetylation (Dompierre et al., 2007; Kim et al., 2016) and detyrosination (Konishi and Setou, 2009), were not altered in *ccp1*$^{-/-}$ neurons (Fig. 1B). This indicated that loss of *Ccp1* alone is sufficient to induce hyperglutamylation in young hippocampal neurons, which could be explained by the relatively low expression of *Ccp6* in cultured hippocampal neurons as compared to adult hippocampus (Fig. S1). We thus aimed at testing if this *ccp1*$^{-/-}$-induced hyperglutamylation is

functionally equivalent to the hyperglutamylation generated by the loss of *Ccp1* and *Ccp6* in its ability to affect axonal transport.

Loss of CCP1 is sufficient to reduce mitochondria transport

To determine if the previously observed reduction of mitochondria motility in *ccp1*$^{-/-}$*ccp6*$^{-/-}$ neurons (Magiera et al., 2018) could be fully reproduced by removing *Ccp1* alone, we crossed *Ccp1*$^{-/+}$ mice, from which we prepared single-embryo primary neuron cultures. This allowed us to obtain both, *ccp1*$^{-/-}$ (hyperglutamylated) and wild-type (control) neurons side-by-side, and measure axonal transport in parallel.

We analysed the movements of mitochondria labelled with the fluorescent dye MitoTracker™ (Fig. 2; S2) as previously done for *ccp1*$^{-/-}$*ccp6*$^{-/-}$ neurons (Magiera et al., 2018). First, we verified that mitochondria densities did not differ in wild-type and *ccp1*$^{-/-}$ neurons (Fig. S2D). Next, we assigned runs, defined as trajectories during which particles move without interruption at constant speed (Fig. 1C; Bodakuntla et al., 2019c). Run length and run speed were quantified, and plotted separately for each experiment to determine medians (Fig. S2A,B). The overall time the entire particle pool spent in movement (overall motility) was determined as the sum of all run durations relative to the overall number of particles in the field (Fig. S2C).

Almost identical to previous measurements in *ccp1*$^{-/-}$*ccp6*$^{-/-}$ neurons (Magiera et al., 2018), tubulin hyperglutamylation generated by loss of *Ccp1* alone (*ccp1*$^{-/-}$) reduced the fraction of time mitochondria spent in movement by about 50% (Fig. 2I) in both, anterograde and retrograde directions without affecting run length or run speed (Fig. 2G,H). These results confirm that hyperglutamylation induced by loss of *Ccp1* alone has the same impact on axonal transport of mitochondria as the double-knockout of *Ccp1* and *Ccp6* (Magiera et al., 2018), and validates *ccp1*$^{-/-}$ neurons as model system to test the effect of hyperglutamylation on the transport of other axonal cargoes.

Hyperglutamylation downregulates motility of lysosomal / endosomal particles

We next aimed at determining the impact of *ccp1*$^{-/-}$-induced hyperglutamylation on the motility of lysosomes, endosomes and autophagosomes. For this, we used two complementary labelling approaches: The fluorescent dye LysoTracker™ (Fig. 3; S3) to label lysosomes but also autophagosomes (Maday et al., 2012), and expression of the lysosome-associated

membrane protein-1 (LAMP1)-GFP (Fig. 4; S4) to label non-degradative lysosomal, as well as endocytic vesicles. Both markers label partially overlapping, but not identical vesicle fractions (Cheng et al., 2018). LysoTracker™ was added to the neurons prior to the transport analyses at DIV4, while LAMP1-GFP was transduced into the cultured neurons at DIV0 using lentiviral vectors (Fig. 1C), resulting in a strong vesicle labelling at DIV4.

We analysed these two markers using the paradigm established for mitochondria (Fig. 1C; 2). Run length and run speed in both, anterograde and retrograde directions were unchanged by hyperglutamylation (*ccp1*$^{-/-}$; Fig. 3G,H; 4G,H). The time spent in movement decreased for both, LysoTracker™-positive (Fig. 3I) and LAMP1-GFP vesicles (Fig. 4I), however to different extents. LAMP1-GFP vesicles showed about 30% less motility in both, anterograde and retrograde directions (Fig. 4I), whereas anterograde movements of LysoTracker™-labelled vesicles were reduced by only about 15% (Fig. 3I).

These observations consistently demonstrate that hyperglutamylation impedes the motility of both vesicle populations. The lower impact on the anterograde motility of LysoTracker™-positive particles might be explained by the low number of anterograde runs observed for this marker (Lee et al., 2011). In contrast, LAMP1, which in the past has been routinely used as a lysosomal marker (Ashrafi et al., 2014; Lee et al., 2011), was recently shown to label both, non-degradative lysosomal and endocytic vesicles (Cheng et al., 2018), which explains the higher number of anterograde transport events (Klinman and Holzbaur, 2016).

Regulation of axonal transport by polyglutamylation is not restricted to kinesin-1-driven cargoes

The anterograde transport of mitochondria, lysosomes and LAMP1-positive endosomes is predominantly driven by motors of the kinesin-1 (KIF5) family. To test if polyglutamylation also impacts transport of cargoes that use different motor proteins, we analysed BDNF vesicles that are transported by a kinesin-3 motor protein, KIF1A (Lo et al., 2011).

BDNF vesicles were visualized by virus-mediated expression of BDNF-mCherry (Fig. 5; S5). As for all other cargoes measured so far, we found that BDNF-mCherry-positive vesicles do not alter run length and run speed in both, anterograde and retrograde directions in hyperglutamylation (*ccp1*$^{-/-}$) conditions (Fig. 5G,H). However, the time spent in movement was reduced by about 50% in anterograde, and about 40% in retrograde direction (Fig. 5I). This strongly suggests that the reduction of the anterograde traffic we had measured for

mitochondria (Fig. 2I) and LAMP1-postitive endosomes (Fig. 4I) is not a specific feature of kinesin-1 motors, but appears to be a more general mechanism that is effective for a range of transport cargoes driven by different motor proteins.

Polyglutamylation specifically affects long runs of BDNF vesicles

As mentioned before, all transport cargos analysed showed similar median run lengths between wild type and *ccp1*$^{-/-}$ neurons (Fig. S2A; S3A; S4A; S5A). However, we noticed that specifically for BDNF vesicles, the greater values, which constitute only a small share of the entire pool of runs, appeared reduced in *ccp1*$^{-/-}$ neurons. To test this possibility, we performed a bin analysis for the run length measurements for each cargo. As we were interested in determining the probability of longer runs, the bin width was chosen about twice the median values (3 µm for anterograde runs of mitochondria and lysosomes; 6 µm for anterograde runs of LAMP1-GFP and BDNF-mCherry vesicles; 5 µm for all retrograde runs; Fig. 6).

Due to strong variation in the longer runs between individual experiments, statistical analyses did not show significant differences, which is why we compared corresponding values for wild-type and *ccp1*$^{-/-}$ neurons for each experimental set (Fig. 6). Strikingly, while mitochondria, lysosomes and LAMP1-positive endosomes showed random patterns in these analyses (Fig. 6A-C), we observed a persistent trend for a decrease in the percentage of long runs for BDNF vesicles in neurons with tubulin hyperglutamylation (*ccp1*$^{-/-}$) in both, anterograde and retrograde directions (Fig. 6D). This unique trend could be related to the transport of BDNF vesicles by KIF1A (Lo et al., 2011), in contrast to KIF5 for the other cargoes.

Indeed, a recent *in vitro* study comparing KIF1A motility on microtubules assembled from Hela and from brain tubulin found a reduced overall run length (defined as the sum of continuous run lengths during a single motility event on the microtubule) of KIF1A on brain microtubules (Lessard et al., 2019), which in contrast to Hela microtubules are polyglutamylated. However, as Hela tubulin differs in several PTMs (Barisic et al., 2015) and tubulin isotypes (Newton et al., 2002) from brain tubulin, conclusive evidence that our observation is directly related to an altered behaviour of KIF1A on hyperglutamylated microtubules is still elusive. Similarly, the increased percentage of longer runs in the retrograde direction cannot be explained by the motor protein dynein, which drives retrograde transport of all here-analysed vesicles. However, dynein can associate with a variety of

adaptor proteins (Reck-Peterson et al., 2018), which might affect the overall transport behaviour of different cargoes in a polyglutamylation-dependent manner.

DISCUSSION

Regulation of axonal transport in neurons is an essential process for neuronal function and homeostasis (Guedes-Dias and Holzbaur, 2019), in which many different cargos need to be delivered to specific locations in a timely manner. Here we analysed the impact of the tubulin PTM polyglutamylation on the axonal transport of cargoes that are functionally and structurally distinct, and that had been previously shown to be differentially regulated under specific physiological conditions (Moutaux et al., 2018; Virlogeux et al., 2018; Zhou et al., 2016). Mitochondria, the main source of cellular ATP, are constantly shuttled in neurons to be docked locally in regions demanding an energy supply, such as the growth cones (Morris and Hollenbeck, 1993) and presynaptic boutons (Lee and Peng, 2008; Rowland et al., 2000). Lysosomes and late endosomes are degradation hubs for misfolded proteins and misfunctioning organelles, which are predominantly transported to the cell body for complete degradation, a process essential for neuronal survival (Pu et al., 2016). BDNF vesicles deliver this neuropeptide to its target sites – synapses - where it controls synaptic plasticity and maturation (Lu et al., 2013). Aberrations of axonal transport can thus lead to severe perturbations in neuronal function and homeostasis, and consequently play key roles in neurodegeneration (Brady and Morfini, 2017; Millecamps and Julien, 2013; Sleigh et al., 2019). Here we show that posttranslational polyglutamylation of neuronal microtubules can regulate the transport of functionally diverse cargoes in hippocampal neurons (Fig. 7A).

How does microtubule polyglutamylation regulate axonal transport?

Axonal transport is regulated at different levels. It is determined (i) by the type of motor proteins that move the cargo, or by additional proteins that are integral parts of transport vesicles/organelles (Hirokawa et al., 2010). Moreover, (ii) cellular MAPs, by binding to the microtubule tracks, can act as ‘road blocks’ for the transport complexes (Vershinin et al., 2007; discussed in Bodakuntla et al., 2019b; Tortosa et al., 2016), or (iii) changes in the overall architecture and integrity of the microtubule cytoskeleton could impact the delivery of cargoes inside neurons (Yogev et al., 2016). PTMs of the microtubule tracks could provide guidance and specificity to different types of transport cargoes, and strikingly, could directly

perturb all of the above-listed transport-regulating mechanisms in case of hyperglutamylation (Fig. 7B).

Emerging data from *in vitro* studies demonstrate that tubulin polyglutamylation can directly interfere with the attachment and processivity of (i) the motor proteins (Sirajuddin et al., 2014), and that different motor proteins show different sensitivity to tubulin glutamylation. Kinesin-3 for instance, which carries BDNF vesicles, was suggested to be sensitive to polyglutamylation (Lessard et al., 2019), which could at least partially explain the stronger impact of hyperglutamylation on BDNF vesicles as compared to LAMP1-vesicles or lysosomes, which are both carried by kinesin-1 (Hirokawa et al., 2010). Previous data have also suggested that (ii) MAPs could be sensitive to tubulin polyglutamylation, in particular the neuronal MAPs tau, MAP2 and MAP1 (Bonnet et al., 2001; Boucher et al., 1994). The differential binding and distribution of MAPs could also affect the (iii) overall architecture of the microtubule cytoskeleton (Harada et al., 1994). For instance, microtubules decorated with neuronal tau or MAP2 show different spacing in neuronal projections (Chen et al., 1992): MAP2, containing longer projection domains, pushes microtubules further apart, and might thus create additional space for the passage of transport cargoes. Microtubule spacing had been indeed shown to control axonal traffic, with consequences on synaptic functions in *Drosophila* neurons (Stephan et al., 2015). Moreover, a link between microtubule spacing, mitochondria transport and tau protein phosphorylation has been established in murine cortical neurons (Shahpasand et al., 2012). At the same time, changes in polyglutamylation could also alter the architecture of the microtubule cytoskeleton by controlling the activity of microtubule-severing enzymes, such as spastin (Lacroix et al., 2010; Valenstein and Roll-Mecak, 2016), which in turn could affect transport. However, our observation that knocking out spastin in *ccp1*$^{-/-}$ mice did not rescue hyperglutamylation-induced degeneration of Purkinje cells (Magiera et al., 2018) suggested that microtubule severing might not be the key molecular defect induced by upregulation of polyglutamylation.

Specificity of transport regulation by polyglutamylation

In hippocampal pyramidal cells used in our study, upregulation of polyglutamylation affected a range of functionally different axonal cargoes, suggesting that polyglutamylation could act as a general traffic control mechanism. However, axonal transport of the same cargoes can be differentially regulated in different types of neurons (Her and Goldstein, 2008). Indeed, a recent study using cerebellar granule cells lacking *Ccp1* found no significant reduction for

endosomal transport in the granule cells with hyperglutamylation (Gilmore-Hall et al., 2019), while at the same time mitochondria transport was perturbed to a similar degree as in hippocampal neurons. While a definite explanation for these differences cannot be given, one possibility is that various polyglutamylases are differentially expressed or active in different neuronal types, and consequently generate distinct patterns of hyperglutamylation upon the deletion of deglutamylases. These distinct patterns would in turn affect different transport cargoes, thus leading to neuron-type specific effects of hyperglutamylation.

The conclusion that transport specificity is controlled by the glutamylating rather than by the deglutamylating enzymes is also supported by our observation that mitochondria transport is similarly reduced in hippocampal neurons lacking *Ccp1* and *Ccp6*, because in both cases the accumulating polyglutamylation is generated by the same set of polyglutamylases in these neurons. It will thus be important to investigate the impact of single polyglutamylases on the transport of different cargoes.

Physiological implications

Notwithstanding the underlying mechanisms, our findings demonstrate that polyglutamylation is a posttranslational mechanism to regulate the transport of a range of neuronal cargoes, and could thus play an important role in controlling vital neuronal functions. Polyglutamylation-related changes in neuronal transport had been previously linked to the delivery of synaptic vesicles (Ikegami et al., 2007), and shown to be activity-dependent (Maas et al., 2009), but direct transport measurements had not been performed. Our analyses thus directly validate these initial findings, and underpin the conceptual idea that by controlling axonal transport (Guedes-Dias and Holzbaur, 2019), polyglutamylation could directly control neuronal activity and eventually memory by controlling synaptic function.

Most importantly, our finding that transport of functionally different cargos is perturbed in neurons with hyperglutamylation strengthens the hypothesis that degeneration of neurons with mutated *Ccp1* (Gilmore-Hall et al., 2019; Magiera et al., 2018; Shashi et al., 2018) could be linked to a dysfunction of intra-neuronal transport in different types of neurons. Understanding the mechanisms of polyglutamylation in the regulation of neuronal homeostasis becomes increasingly relevant as more and more reports link mutations in deglutamylases to human neurodegenerative disorders (Karakaya et al., 2019; Shashi et al., 2018; Sheffer et al., 2019; Velez et al., 2016).

Conclusions

Together, the results of our analyses highlight the emerging role of tubulin polyglutamylation as a key regulator of neuronal transport, and its perturbation as a causative factor for neurodegenerative disorders. An intriguing question to be addressed in the future is how polyglutamylation relates to other tubulin PTMs that are also present in neurons, such as detyrosination and acetylation, both of them known to also affect transport (Dompierre et al., 2007; Kim et al., 2016; Konishi and Setou, 2009). Our gene expression analyses (Fig. S1) show that enzymes involved in tubulin detyrosination and acetylation are at their highest expression levels in the young, undifferentiated neurons. In contrast, enzymes involved in polyglutamylation show an increasing expression throughout development, and persistent expression into adulthood. This strongly suggests that polyglutamylation, by remaining particularly dynamic in adult neurons, plays a central role in adapting cargo transport to physiological requirements and activity of neurons throughout life, thus assuring neuronal homeostasis.

Materials and Methods

Mouse lines

All the animals in this study were used in accordance with the recommendations of the European Community (2010/63/UE). Experimental procedures were specifically approved by the ethics committee of the Institut Curie CEEA-IC #118 (authorization n°*04395.03* given by National Authority) in compliance with the international guidelines.

Generation of *ccp1*$^{-/-}$ and *Ccp1*$^{flox/flox}$*Ccp6*$^{flox/flox}$ mice was described in detail before (Magiera et al., 2018; Munoz-Castaneda et al., 2018). All embryos and mice, both male and female, were used for the transport analyses.

Genotyping

For adult mice, DNA was extracted from ear fragments (collected during identification of mice) or tail fragments by proteinase-K digestion. Lysis buffer (0.1 M Tris-HCl pH 8 (Sigma #T1503), 0.2 M NaCl (Sigma #S3014), 5 mM EDTA (Euromedex #EU0007-C) and 0.4% SDS (Euromedex #EU0660)) containing 0.1 mg/ml proteinase K (#193504, MP Biomedicals) was added to the sample, incubated at 56°C for 4 h and 10 min at 95°C. For hippocampal neuron cultures, a piece of the brain tissue from the E17.5-embryos was lysed using REDExtract-N-Amp™ Tissue PCR Kit (Sigma #XNAT) using manufacturer's instructions. PCR-based genotyping was carried out using the primers and protocols described in our earlier studies (Bodakuntla et al., 2019a; Magiera et al., 2018).

RNA isolation and RT-qPCR

Total RNA from mouse hippocampal neurons cultured for 1, 4, 7 or 10 days, as well as entire hippocampi from mice of different ages was isolated using the Trizol reagent (Life technologies) using manufacturer's instructions. Concentrations and quality of the extracted RNA was determined with a Nanodrop Spectrophotometer (Thermo Fisher Scientific). cDNA for these RNAs were synthesized with the SYBRGreen Master Mix kit. PCR amplification was performed on an ABI Prism 7900 Sequence Detection System (Perkin-Elmer Applied Biosystems, Foster City, CA) as described in detail elsewhere (Bieche et al., 1999). Reverse transcription real-time quantitative PCR (RT-qPCR) was performed for all the known tubulin-modifying enzymes, β3-tubulin (TUBB3) and for the TATA-binding protein (*Tbp*) gene

(NM_013684), which was used as a control. PCR conditions are available upon request. The relative mRNA expression levels were represented as the N-fold difference in target gene expression relative to the *Tbp* gene (termed 'N_{target}') and calculated as $N_{target} = 2^{\Delta Ctsample}$. The value of the cycle threshold (ΔCt) of a given sample was determined by subtracting the average Ct value of the target gene from the average Ct value for the *Tbp* gene. Primers used in this study are shown in Table S1.

Sample preparation and immunoblotting

Hippocampal neurons transduced on DIV4 (4 days in vitro). Wild type, *Ccp1*$^{-/+}$, *ccp1*$^{-/-}$, or *Ccp1*$^{flox/flox}$*Ccp6*$^{flox/flox}$ transduced with lentivirus encoding GFP or GFP-2A-cre were collected in 2x Laemmli buffer (180 mM DTT (Sigma #D9779), 4% SDS (VWR #442444H), 160 mM Tris-HCl pH 6.8, 20% glycerol (VWR #24388.295), bromophenol blue) buffer. The samples were then boiled at 95°C for 5 min, spun down at 20,000×g for 5 min using a table top centrifuge, and stored at -20°C. Samples were loaded on SDS-PAGE gels, separated and transferred onto a nitrocellulose membrane using Biorad Trans-Blot® Turbo system, according to manufacturer's instructions. The membranes were incubated with an anti-α-tubulin antibody (12G10, 1/1,000 (vol/vol); developed by J. Frankel and M. Nelson, obtained from the Developmental Studies Hybridoma Bank, developed under the auspices of the NICHD, and maintained by the University of Iowa), and an anti-polyglutamylated tubulin antibody (polyE, 1/10,000 (vol/vol); AdipoGen #AG-25B-0030) to determine differences in tubulin polyglutamylation at equal tubulin levels. Chemiluminescence signal on the membrane was revealed using Clarity™ Western ECL Substrate (Biorad #1705060) solution.

Mouse hippocampal neuron cultures

Hippocampal neuron cultures were performed according to standard protocols described earlier (Bodakuntla et al., 2019a; Kaech and Banker, 2006). Briefly, pregnant mice at 17.5 days of gestation were sacrificed using cervical dislocation, the embryos were decapitated and hippocampi of individual embryos were collected in separate tubes. At the same time, a piece of brain tissue of the individual embryos was collected, subjected to lysis using REDExtract-N-Amp™ Tissue PCR Kit (Sigma #XNAT) and analyzed for the *Ccp1* gene. Collected hippocampi were enzymatically and mechanically dissociated using trypsin and fire-polished Pasteur-pipettes, respectively. Based on the genotyping results, only wild type and *ccp1*$^{-/-}$

hippocampal neurons were counted and plated on poly-D-lysine (#354210, Corning) coated plastic dishes for immunoblot analysis or on glass-bottom dishes (#81158, Ibidi) for live cell imaging (transport analysis). A schematic representation of the work flow is given in Fig. 1C.

Cloning and DNA plasmids

Cre-recombinase and vesicle markers (LAMP1) were cloned in to pTRIP lentiviral vectors using sequence- and ligation-independent cloning (Jeong et al., 2012), which was described in detail in our earlier studies (Bodakuntla et al., 2019a). Briefly, cre-recombinase was amplified using primers with at least 15 bp of homology sequence to the ends of the target vector and inserted in the pTRIP vector with CMV-enhanced chicken beta-actin (CAG) promoter at the XhoI site. The cre-recombinase was cloned after a self-cleavable 2A peptide sequence (Kim et al., 2011) which was in frame with the GFP. The *Lamp1* gene, a marker for late endosomes, was inserted at the NheI site, creating a C-terminally GFP-tagged protein. Primers used for amplification of cre-recombinase and *Lamp1* are given below. NLS-cre-FS-2A: 5'-tccactagtgtcgacATGCCCAAGAAGAAGAGGAAGGTG-3', NLS-cre-FS-2A: 5'-catgtttttctaggtTAATCGCCATCTTCCAGCAGGC-3', mLAMP1-FS1: 5'-agaattattccgctagcATGGCGGCCCCCGGCGCCCGGCG-3', mLAMP1-RS1: 5'-accatGGTGGCgctagcGATGGTCTGATAGCCGGCGTGACTCC-3'. Packaging plasmids psPAX2 and pCMV-VSVG are gifts from D. Trono (Addgene plasmid #12260) and B. Weinberg (Addgene plasmid #8454), respectively. BDNF-mCherry was a kind gift from F. Saudou, Grenoble Institute of Neurosciences (GIN), France.

Lentivirus production and transduction

Lentivirus particles were produced using protocols described earlier (Bodakuntla et al., 2019a). Briefly, X-Lenti 293T cells (#632180; Takara) plated in 6-well plates were co-transfected with 1.6 µg plasmid of interest and packaging plasmids (0.4 µg of pCMV-VSVG and 1.6 µg of psPAX2) using 8 µl of TransIT-293 (#MIR 2705, Mirus Bio) transfection reagent per well. On the next day, the culture medium was changed to Neurobasal medium (Thermo Fisher #21103049) supplemented with 1× Penicillin-Streptomycin (Life Technologies #15140130). Next day, the virus-containing supernatants were harvested, passed through a 0.45 µm filter and either used fresh or aliquoted and stored at -80°C. To determine the optimal amount of virus for transduction, lentivirus aliquots were thawed, and

different volumes were added to cultured primary neurons. Based on the expression levels of the GFP protein, the desired amount of virus to achieve maximum transduction efficiency was determined. On DIV0, *Ccp1*$^{flox/flox}$*Ccp6*$^{flox/flox}$ hippocampal neurons were either left untransduced for controls, or transduced with lentiviruses encoding for GFP alone (control), or GFP-2A-cre-recombinase in order to transform the flox genes into knockouts. For transport experiments, wild-type and *ccp1*$^{-/-}$ neurons were transduced with lentiviruses encoding either LAMP1-GFP or BDNF-mCherry.

Imaging of axonal transport

Transport assays and analysis paradigms were designed based on established protocols (Ghiretti et al., 2016; Klinman and Holzbaur, 2016) and are described in detail earlier (Bodakuntla et al., 2019c). Briefly, for all transport experiments, neurons were imaged on DIV4. For imaging mitochondria or lysosomes movements in the axon, neurons were incubated with 2 nM MitoTracker™ Red CMXRos (Thermo Fisher #M7512) for 1 min or 100 nM LysoTracker™ Red DND-99 (Thermo Fisher #L7528) for 30 min in the cell culture incubator, respectively. After the staining, neurons are washed once with conditioned medium. Conditioned medium is neurobasal medium containing 1× B27 (Thermo Fisher #17504044) and 1× GlutaMax (Thermo Fisher #35050038) is taken from untreated DIV4 neurons.

For imaging LAMP1-GFP and BDNF-mCherry vesicles, DIV0 neurons were transduced with lentivirus encoding LAMP1-GFP and BDNF-mCherry, differentiated until DIV4, and washed once with conditioned medium before imaging. Particle movements were immediately imaged using a Nikon Ti-E spinning disk inverted confocal laser microscope equipped with a 60× oil-immersion objective (N.A. 1.40). Images were captured using an ORCA-Flash 4.0 camera (Hamamatsu) set at 2×2 binning, and operated through Leica MM AF imaging software. All particle movements were recorded every 300 ms for 1 min in stream mode, with imaging chamber set at 37°C and 5% CO_2. For each experiment, at least five neurons per treatment group were imaged, without exceeding 30 min of imaging time per dish. A schematic representation of the work flow is given in Fig. 1C.

Quantification of axonal transport

All the image processing and transport analysis procedures were described in detail elsewhere (Bodakuntla et al., 2019c). All the data analyses were performed using ImageJ 1.47v with

KymoToolBox plugin (Zala et al., 2013) (available upon request from F. Cordelières, Bordeaux Imaging Center, France). Refer to https://github.com/fabricecordelieres/IJ_KymoToolBox for detailed explanation of the plugin. For each movie, a maximum-intensity projection of the time lapse movie was generated, and the paths of particles movements along the longest neurite - the axon - were manually traced. The KymoToolBox plugin was used to generate kymostacks (straightened videos of particle movements in the axons; suppl. Movies S1-S4, lower panels) and kymographs calibrated in x-axis (distance in µm) and y-axis (time in seconds; Fig. 2B; 3B; 4B; 5B). The kymographs were then analysed by manually tracing each distinct run of a particle's trajectory using the segmented line tool from ImageJ. In our analyses, a 'run' was defined as the continuous movement of a given particle without changes in speed or direction. Runs with speeds lower than 0.10 µm/s, or shorter than 0.9 µm (corresponds to 5 pixels in our system and equivalent to an average size of the particles imaged) were not considered. To distinguish two consecutive runs in the same direction, we first traced a linear slope for the entire trajectory. If this linear trace did not follow the initial trajectory of the particle (minimum offset: 3 pixels corresponding to ~0.5 µm), we defined a novel run with a different trajectory. While we are aware that some trajectories leave the imaging windows, we still included them in our analyses. Considering that our readouts are comparisons between wild type and *ccp1*$^{-/-}$ neurons, eventual biases introduced by this analysis paradigm will equally be present in both conditions, and thus not significantly influence the final results. The plugin generates a kymograph highlighting the anterograde runs in green, retrograde runs in red and immotile trajectories in blue (kymographs of one experiment shown in Fig. 2B; 3B; 4B; 5B). A schematic representation of the work flow is given in Fig. 1C.

Transport parameters run length and run time were measured as shown in Fig. 1C, and run speed and overall motility were calculated (Fig. S2; S3; S4; S5). For each experiment, run length and run speed distributions from each condition were plotted and medians of the distributions were compared. Overall motility, percentage of time particles spend in movement in the given observation time is calculated for each condition. A motility of 100% means that all detected particles in the kymograph were in movement for the whole duration of observation time (60 s).

$$Overall\ motility\ [\%] = \frac{Sum\ of\ all\ run\ times\ in\ kymograph: \sum T1 \ldots Tn\ [s] \times 100}{Number\ of\ particles\ in\ kymograph \times Imaging\ time\ [s]}$$

Particle density is calculated as the number of particles per length of the axon. The 'average run length' (Fig. 2G; 3G; 4G; 5G) and 'average run speed' (Fig. 2H; 3H; 4H; 5H) were determined by calculating the mean of all medians (Fig. S2; S3; S4; S5). The 'average overall motility' (Fig. 2I; 3I; 4I; 5I) and 'average vesicle density' (Fig. 2J; 3J; 4J; 5J) were determined by calculating the mean of the respective values from all the experiments (Fig. S2; S3; S4; S5). Bin analyses was performed to determine the probability of longer vesicle run. Bin width was set approximately twice the median values – 3 μm for anterograde runs of mitochondria and lysosomes; 6 μm for anterograde runs of LAMP1-GFP and BDNF-mCherry vesicles; 5 μm for all retrograde runs (Fig. 6).

Statistical analyses

qPCR analysis for tubulin-modifying enzymes was performed in samples collected from three independent experiments. The analyses for all the samples in an experiment were performed simultaneously in a single qPCR run. Data obtained from three independent experiments was represented as bar graphs showing mean ±SD (Fig. S1).

For statistical analyses of transport parameters, values for run length and speed of a single experiment were represented as scatter plots with a line indicating a median and whiskers at interquartile ranges (25^{th} and 75^{th} percentiles; Fig. S2A,B; S3A,B; S4A,B; S5A,B). Fraction of time spent in movement (overall motility) and particle density in the axon were calculated and represented as bar graphs (Fig. S2C,D; S3C,D; S4C,D; S5C,D). All experiments have been performed at least in triplicates. Medians of the run length and speed distributions from all the experiments were averaged, and shown as bar graphs of mean ±SEM (Fig. 2G,H; 3G,H; 4G,H; 5G,H). Overall motility and particle densities calculated in individual experiments was averaged and shown as bar graphs of mean±SEM (Fig. 2I,J; 3I,J; 4I,J; 5I,J). Statistical significance for particle densities was tested using Mann-Whitney test, and p-values were given. Statistical significance for average run length, average speed and average overall motility was tested using Two-way ANOVA with a post-hoc by Bonferroni multiple comparison test, and p values are given. Statistical significance for qPCR analyses shown in Fig. S1 was tested using One-way ANOVA with a post-hoc by Bonferroni multiple comparison test, and p values are given. All the numerical values used for quantification of axonal transport are shown in Table S2.

Acknowledgement

This work was supported by the ANR-10-IDEX-0001-02, the LabEx CelTisPhyBio ANR-11-LBX-0038. CJ is supported by the Institut Curie, the French National Research Agency (ANR) awards ANR-12-BSV2-0007 and ANR-17-CE13-0021, the Institut National du Cancer (INCA) grant 2014-PL BIO-11-ICR-1, and the Fondation pour la Recherche Medicale (FRM) grant DEQ20170336756. MMM is supported by the EMBO short-term fellowship ASTF 148-2015 and by the Fondation Vaincre Alzheimer grant FR-16055p, and SB by the FRM grant FDT201805005465. SB, CV, CG-B and CJ are supported by the Evaluación y Orientación de la Cooperación Científica - Comisión Nacional de Investigación Científica y Tecnológica (ECOS-CONICYT; grant C14B01).

We thank C. Alberti, E. Belloir, F. Bertrand, G. Buhagiar, C. Caspersen, V. Dangles-Marie, S. Gadadhar, I. Grandjean, H. Hermange, F. Maksut, C. Serieyssol, M. Sittewelle, A. Thadal, A. Zeggai (Institut Curie) for technical assistance. We are grateful to M.-N. Soler, C. Lovo and L. Besse from the PICT-IBiSA@Orsay Imaging Facility of the Institut Curie supported by the ANR through the "Investment for the future" program (France-BioImaging, ANR-10-INSB-04), and to N. Manel (Institut Curie, Paris) for material and advice for the lentivirus production, and F. Saudou for providing essential material. We would like to thank F.P. Cordelières (Bordeaux Imaging Center, France) for the KymoToolBox plugin, as well as M. Brill (Technical University Munich, Germany), R. Chabrier, F. Del Bene, V. Marthiens (Institut Curie) for instructive discussions and advice.

Author contributions

conceptualization: S. Bodakuntla, C. Janke and M.M. Magiera; methodology: S. Bodakuntla, A. Schnitzler, C. Villablanca, I. Bieche, C. Janke and M.M. Magiera; validation: S. Bodakuntla, A. Schnitzler, I. Bieche, C. Janke and M.M. Magiera; formal analysis: S. Bodakuntla, A. Schnitzler, C. Villablanca, I. Bieche, C. Janke and M.M. Magiera; investigation: S. Bodakuntla, A. Schnitzler, C. Janke and M.M. Magiera; writing, original draft: S. Bodakuntla, C. Janke and M.M. Magiera; writing, review and editing: S. Bodakuntla, C. Janke and M.M. Magiera; visualization: S. Bodakuntla, I. Bieche, C. Janke and M.M. Magiera; supervision: C. Gonzalez-Billault, I. Bieche, C. Janke and M.M. Magiera; project administration: C. Janke and M.M. Magiera; funding acquisition: S. Bodakuntla, C. Gonzalez-Billault, C. Janke and M.M. Magiera.

Figure Legends

Figure 1: Using *Ccp1*$^{-/-}$ neurons to determine the impact of tubulin hyperglutamylation in neurons.

(A) Immunoblot of cell extracts of DIV4 *Ccp1*$^{flox/flox}$*Ccp6*$^{flox/flox}$ hippocampal neurons either untransduced, or transduced with lentiviruses encoding GFP or GFP-2A-cre, and hippocampal neurons from wild type, *Ccp1*$^{-/+}$ and *ccp1*$^{-/-}$ embryos probed with an anti-polyglutamylation antibody (polyE). α-tubulin levels, detected with the 12G10 antibody, were used as a control for tubulin load. Note that polyglutamylation levels are increased similarly in neurons transduced with GFP-2A-cre lentivirus and in neurons lacking *Ccp1* (*ccp1*$^{-/-}$), indicating that removal of *Ccp1* alone is sufficient to induce hyperglutamylation. **(B)** Hippocampal neurons from wild type, *Ccp1*$^{-/+}$ and *ccp1*$^{-/-}$ embryos probed with an anti-polyglutamylation (polyE), anti-detyrosination (detyr-tubulin), anti-acetylation (6-11-B1), and α-tubulin (12G10) antibodies. Note that neither detyrosination, nor acetylation change in *ccp1*$^{-/-}$ neurons. **(C)** Experimental flow scheme for the transport experiments shown in Fig. 2-5. *Ccp1*$^{-/+}$ mice were bred and hippocampi from E17.5 embryos were collected separately for neuronal cultures. In parallel, tissue samples of each embryo were collected and the *Ccp1* genotype determined. Based on the genotyping result, hippocampal neurons from wild type and *ccp1*$^{-/-}$ embryos were cultured separately. For analysing LAMP1 and BDNF particle transport, lentiviruses particles were added to the neurons on DIV0. For analysing mitochondria and lysosomes transport, neurons were treated with MitoTracker™ and LysoTracker™ prior to imaging. On DIV4, when the neurons are polarized with a distinct axon, the movements of fluorescently labelled cargoes in at least five wild-type and *ccp1*$^{-/-}$ neurons were recorded for 1 min. Groups of wild-type and *ccp1*$^{-/-}$ neurons that were prepared on the same day were analysed together as one experiment (single experiments represented in Fig. S2; S3; S4; S5). differentiated neurons were imaged and the particle movement was analysed by hand-tracing the longest neurite of each recorded neuron, i.e. the axon. A kymograph was generated, and each particle path was fragmented into single runs of constant speed. How single runs were determined is described in detail in materials and methods. We then extracted several parameters such as run length (L), run time (T), and calculated run speed (L/T), fraction of time spent in motility and particle density for each cargo type. The results of one complete, representative experiment, as well as all kymographs, are shown in the main figures (Fig. 2A-F; 3A-F; 4A-F; 5A-F). We next plot the average of all median values of the independent experiments (Fig. S2; S3; S4;

S5) for run speed and run length (Fig. 2G,H; 3G,H; 4G,H; 5G,H), as well as the average values of time spent in movement (Fig. 2I; 3I; 4I; 5I) and particle densities (Fig. 2J; 3J; 4J; 5J).

Figure 2. Increased tubulin polyglutamylation in *ccp1*$^{-/-}$ neurons reduces the overall motility of mitochondria.

Analysis of mitochondria movements in wild type vs. *ccp1*$^{-/-}$ neurons. At DIV4, mitochondria stained with MitoTracker™ were imaged in the longest extension (axon) of the neuron. Mitochondria movements were recorded for 1 min using a spinning-disk microscope. **(A)** Representative images (inverted grey scale) of one neuron per genotype stained with MitoTracker™ (suppl. Movie S1, upper panels). Scale bars: 20 µm. **(B)** Kymographs of mitochondria movements for all neurons analysed within one single experiment (exp. 1; corresponding kymostacks are shown in suppl. Movie S1, lower panels). Each run is defined as a continuous movement of the mitochondria without change in direction or speed. Anterograde and retrograde runs are color-coded in green and red, respectively, while immotile events are shown in blue. Scale bars: 60 s, 20 µm. **(C) – (F)** Analyses of one single experiment (exp. 1; panel B) for **(C)** run length and **(D)** run speed of mitochondria shown as scatter plots where each point represents the value of a single run. The horizontal black line indicates the median of the distribution with whiskers at interquartile range. Numerical value of the medians is indicated below respective distributions. Light green circles are for wild type and dark green circles are for *ccp1*$^{-/-}$. Filled circles are for anterograde and open circles are for retrograde direction. **(E)** Fraction of time spent in motility (overall motility) and **(F)** mitochondrial density from this experiment are represented as bar graphs. **(G) – (J)** Statistical analyses of four independent experiments (each of them shown separately in Fig. S2): average **(G)** run length, **(H)** run speed, **(I)** overall motility and **(J)** mitochondrial density are shown as bar graphs ±SEM. Filled bars show anterograde, and open bars retrograde movements. Light green bars are for wild type and dark green bars are for *ccp1*$^{-/-}$ neurons.

Figure 3. Increased tubulin polyglutamylation reduces the overall motility of lysosomes.

Analysis of lysosomes movements in wild type vs. *ccp1*$^{-/-}$ neurons. At DIV4, lysosomes movements labelled with LysoTracker™ were imaged in the axon for 1 min using a spinning-disk microscope. **(A)** Representative images (inverted grey scale) of one neuron per genotype stained with LysoTracker™ (suppl. Movie S2, upper panels). Scale bars: 20 µm. **(B)** Kymographs of lysosomes movements for all neurons analysed within one single experiment (exp. 1; all corresponding kymostacks are shown in suppl. Movie S2, lower panels). Scale bars: 60 s, 20 µm. **(C) – (F)** Analyses of one single experiment (exp. 1; panel B) for **(C)** Run length and **(D)** run speed of lysosomes shown as scatter plots as shown in Fig. 2, where each point represents the value of a single run. Light orange colour circles are for wild type and dark orange colour circles are for *ccp1*$^{-/-}$. Filled circles are for anterograde and open circles are for retrograde direction. **(E)** Fraction of time spent in motility (overall motility) and **(F)** lysosome density from this experiment are represented as bar graphs. **(G) – (J)** Statistical analyses of four independent experiments (each of them shown separately in Fig. S3): average **(G)** run length, **(H)** run speed, **(I)** overall motility and **(J)** lysosome density are shown as bar graphs ±SEM. Filled bars show anterograde, and open bars retrograde movements. Light orange colour bars are for wild type and dark orange colour bars are for *ccp1*$^{-/-}$ neurons.

Figure 4. Increased tubulin polyglutamylation reduces the overall motility of LAMP1 endosomes.

Analysis of LAMP1-positive endosome movements in wild type vs. *ccp1*$^{-/-}$ neurons. Neurons were transduced with LAMP1-GFP lentivirus at DIV0, and movements of LAMP1-positive particles were imaged at DIV4 for 1 min using a spinning-disk microscope. **(A)** Representative images (inverted grey scale) of one neuron per genotype expressing LAMP1-GFP (suppl. Movie S3, upper panels). Scale bars: 20 µm. **(B)** Kymographs of LAMP1-endosome movements for all neurons analysed within one single experiment (exp. 1; all corresponding kymostacks are shown in suppl. Movie S3, lower panels). Scale bars: 60 s, 20 µm. **(C) – (F)** Analyses of one single experiment (exp. 1; panel B) for **(C)** Run length and **(D)** run speed of LAMP1 endosomes shown as scatter plots as shown in Fig. 2, where each point represents the value of a single run. Light blue circles are for wild type and dark blue circles are for *ccp1*$^{-/-}$. Filled circles are for anterograde and open circles are for retrograde direction. **(E)** Fraction of time spent in motility (overall motility) and **(F)** LAMP1 endosome density from this experiment are represented as bar graphs. **(G) – (J)** Statistical analyses of

three independent experiments (each of them shown separately in Fig. S4): average **(G)** run length, **(H)** run speed, **(I)** overall motility and **(J)** LAMP1 endosome density are shown as bar graphs ±SEM. Filled bars show anterograde, and open bars retrograde movements. Light blue bars are for wild type and dark blue bars are for *ccp1*$^{-/-}$ neurons.

Figure 5. Increased tubulin polyglutamylation reduces the overall motility of BDNF vesicles.

Analysis of BDNF vesicle movements in wild type vs. *ccp1*$^{-/-}$ neurons. Neurons were transduced with BDNF-mCherry lentivirus at DIV0, and movements of BDNF-positive particles were imaged at DIV4 for 1 min using a spinning-disk microscope. **(A)** Representative images (inverted grey scale) of one neuron per genotype expressing BDNF-mCherry (suppl. Movie S4, upper panels). Scale bars: 20 µm. **(B)** Kymographs of BDNF-vesicle movements for all neurons analysed within one single experiment (exp. 1; all corresponding kymostacks are shown in suppl. Movie S4, lower panels). Scale bars: 60 s, 20 µm. **(C) – (F)** Analyses of one single experiment (exp. 1; panel B) for **(C)** Run length and **(D)** run speed of BDNF vesicles shown as scatter plots as shown in Fig. 2, where each point represents the value of a single run. Light purple circles are for wild type and dark purple circles are for *ccp1*$^{-/-}$. Filled circles are for anterograde and open circles are for retrograde direction. **(E)** Fraction of time spent in motility (overall motility) and **(F)** BDNF-vesicle density from this experiment are represented as bar graphs. **(G) – (J)** Statistical analyses of three independent experiments (each of them shown separately in Fig. S5): average **(G)** run length, **(H)** run speed, **(I)** overall motility and **(J)** BDNF-vesicle density are shown as bar graphs ±SEM. Filled bars show anterograde, and open bars retrograde movements. Light purple bars are for wild type and dark purple bars are for *ccp1*$^{-/-}$ neurons.

Figure 6. Tubulin hyperglutamylation affects long runs of BDNF vesicles

(A-D) Bin analyses of anterograde and retrograde run lengths of **(A)** mitochondria, **(B)** lysosomes, **(C)**, LAMP1-GFP and **(D)** BDNF-mCherry vesicles were performed to determine the probability of long runs in wild type vs. *ccp1*$^{-/-}$ neurons. The bin values, defined as twice the median value of the run length distributions were: 3 µm for anterograde runs of

mitochondria and lysosomes, 6 µm for anterograde runs of LAMP1-GFP and BDNF-mCherry vesicles; 5 µm for all retrograde runs. Pairs of connected points represent values from wild type and *ccp1*$^{-/-}$ conditions from the same experiments.

Figure 7. Tubulin hyperglutamylation reduces the overall motility of all cargoes analysed

(A) Bar graphs representing the relative amount of time different vesicles spent in anterograde (filled bars) and retrograde (open bars) in *ccp1*$^{-/-}$ neurons. Note that mitochondria and BDNF vesicles show the strongest decrease of motility in *ccp1*$^{-/-}$ neurons.

(B) Schematic representation of possible mechanisms by which tubulin polyglutamylation could regulate axonal transport, and the predicted impacts of hyperglutamylation. Excessive levels of polyglutamylation (red tails on the microtubules) could affect the switching of cargoes between microtubule tracks, which is a rate limiting factor for efficient transport (Yogev et al., 2016). Hyperglutamylation could also cause frequent detachment of cargoes from the microtubule tracks, either indirectly by disrupting microtubules (Lacroix et al., 2010; Valenstein and Roll-Mecak, 2016), by abnormal accumulation of MAPs (Vershinin et al., 2007) that could act as 'roadblocks', or directly by modulating the affinity of motor proteins to the microtubule tracks (Sirajuddin et al., 2014).

References

Aillaud, C., Bosc, C., Peris, L., Bosson, A., Heemeryck, P., Van Dijk, J., Le Friec, J., Boulan, B., Vossier, F., Sanman, L. E. et al. (2017). Vasohibins/SVBP are tubulin carboxypeptidases (TCPs) that regulate neuron differentiation. *Science* **358**, 1448-1453.

Akella, J. S., Wloga, D., Kim, J., Starostina, N. G., Lyons-Abbott, S., Morrissette, N. S., Dougan, S. T., Kipreos, E. T. and Gaertig, J. (2010). MEC-17 is an alpha-tubulin acetyltransferase. *Nature* **467**, 218-22.

Alexander, J. E., Hunt, D. F., Lee, M. K., Shabanowitz, J., Michel, H., Berlin, S. C., MacDonald, T. L., Sundberg, R. J., Rebhun, L. I. and Frankfurter, A. (1991). Characterization of posttranslational modifications in neuron-specific class III beta-tubulin by mass spectrometry. *Proc Natl Acad Sci U S A* **88**, 4685-9.

Ashrafi, G., Schlehe, J. S., LaVoie, M. J. and Schwarz, T. L. (2014). Mitophagy of damaged mitochondria occurs locally in distal neuronal axons and requires PINK1 and Parkin. *J Cell Biol* **206**, 655-70.

Barisic, M., Silva e Sousa, R., Tripathy, S. K., Magiera, M. M., Zaytsev, A. V., Pereira, A. L., Janke, C., Grishchuk, E. L. and Maiato, H. (2015). Microtubule detyrosination guides chromosomes during mitosis. *Science* **348**, 799-803.

Bentley, M. and Banker, G. (2016). The cellular mechanisms that maintain neuronal polarity. *Nat Rev Neurosci* **17**, 611-22.

Bieche, I., Onody, P., Laurendeau, I., Olivi, M., Vidaud, D., Lidereau, R. and Vidaud, M. (1999). Real-time reverse transcription-PCR assay for future management of ERBB2-based clinical applications. *Clin Chem* **45**, 1148-56.

Bodakuntla, S., Janke, C. and Magiera, M. M. (2019a). Knocking out multiple genes in cultured primary neurons to study tubulin posttranslational modifications. *Methods in Molecular Biology*, in press.

Bodakuntla, S., Jijumon, A. S., Villablanca, C., Gonzalez-Billault, C. and Janke, C. (2019b). Microtubule-Associated Proteins: Structuring the Cytoskeleton. *Trends Cell Biol* **29**, 804-819.

Bodakuntla, S., Magiera, M. M. and Janke, C. (2019c). Determining the role of tubulin posttranslational modifications on axonal transport. *Methods in Molecular Biology*, in press.

Bonnet, C., Boucher, D., Lazereg, S., Pedrotti, B., Islam, K., Denoulet, P. and Larcher, J. C. (2001). Differential binding regulation of microtubule-associated proteins MAP1A, MAP1B, and MAP2 by tubulin polyglutamylation. *J Biol Chem* **276**, 12839-12848.

Boucher, D., Larcher, J. C., Gros, F. and Denoulet, P. (1994). Polyglutamylation of tubulin as a progressive regulator of in vitro interactions between the microtubule-associated protein Tau and tubulin. *Biochemistry* **33**, 12471-12477.

Brady, S. T. and Morfini, G. A. (2017). Regulation of motor proteins, axonal transport deficits and adult-onset neurodegenerative diseases. *Neurobiol Dis* **105**, 273-282.

Brants, J., Semenchenko, K., Wasylyk, C., Robert, A., Carles, A., Zambrano, A., Pradeau-Aubreton, K., Birck, C., Schalken, J. A., Poch, O. et al. (2012). Tubulin Tyrosine

Ligase Like 12, a TTLL Family Member with SET- and TTL-Like Domains and Roles in Histone and Tubulin Modifications and Mitosis. *PLoS ONE* **7**, e51258.

Cavanagh, J. B. (1984). The problems of neurons with long axons. *Lancet* **1**, 1284-7.

Chen, J., Kanai, Y., Cowan, N. J. and Hirokawa, N. (1992). Projection domains of MAP2 and tau determine spacings between microtubules in dendrites and axons. *Nature* **360**, 674-7.

Cheng, X.-T., Xie, Y.-X., Zhou, B., Huang, N., Farfel-Becker, T. and Sheng, Z.-H. (2018). Characterization of LAMP1-labeled nondegradative lysosomal and endocytic compartments in neurons. *J Cell Biol* **217**, 3127-3139.

Choquet, D. and Triller, A. (2013). The dynamic synapse. *Neuron* **80**, 691-703.

Conde, C. and Caceres, A. (2009). Microtubule assembly, organization and dynamics in axons and dendrites. *Nat Rev Neurosci* **10**, 319-32.

DeFelipe, J. (2013). Cajal and the discovery of a new artistic world: the neuronal forest. *Prog Brain Res* **203**, 201-20.

Dompierre, J. P., Godin, J. D., Charrin, B. C., Cordelieres, F. P., King, S. J., Humbert, S. and Saudou, F. (2007). Histone deacetylase 6 inhibition compensates for the transport deficit in Huntington's disease by increasing tubulin acetylation. *J Neurosci* **27**, 3571-83.

Eddé, B., Rossier, J., Le Caer, J. P., Desbruyeres, E., Gros, F. and Denoulet, P. (1990). Posttranslational glutamylation of alpha-tubulin. *Science* **247**, 83-85.

Ghiretti, A. E., Thies, E., Tokito, M. K., Lin, T., Ostap, E. M., Kneussel, M. and Holzbaur, E. L. F. (2016). Activity-Dependent Regulation of Distinct Transport and Cytoskeletal Remodeling Functions of the Dendritic Kinesin KIF21B. *Neuron* **92**, 857-872.

Gilmore-Hall, S., Kuo, J., Ward, J. M., Zahra, R., Morrison, R. S., Perkins, G. and La Spada, A. R. (2019). CCP1 promotes mitochondrial fusion and motility to prevent Purkinje cell neuron loss in pcd mice. *J Cell Biol* **218**, 206-219.

Guedes-Dias, P. and Holzbaur, E. L. F. (2019). Axonal transport: Driving synaptic function. *Science* **366**, science.aaw9997.

Harada, A., Oguchi, K., Okabe, S., Kuno, J., Terada, S., Ohshima, T., Sato-Yoshitake, R., Takei, Y., Noda, T. and Hirokawa, N. (1994). Altered microtubule organization in small-calibre axons of mice lacking tau protein. *Nature* **369**, 488-91.

Her, L.-S. and Goldstein, L. S. B. (2008). Enhanced sensitivity of striatal neurons to axonal transport defects induced by mutant huntingtin. *J Neurosci* **28**, 13662-72.

Hirokawa, N., Niwa, S. and Tanaka, Y. (2010). Molecular motors in neurons: transport mechanisms and roles in brain function, development, and disease. *Neuron* **68**, 610-38.

Ikegami, K., Heier, R. L., Taruishi, M., Takagi, H., Mukai, M., Shimma, S., Taira, S., Hatanaka, K., Morone, N., Yao, I. et al. (2007). Loss of alpha-tubulin polyglutamylation in ROSA22 mice is associated with abnormal targeting of KIF1A and modulated synaptic function. *Proc Natl Acad Sci U S A* **104**, 3213–3218.

Ikegami, K., Mukai, M., Tsuchida, J.-i., Heier, R. L., Macgregor, G. R. and Setou, M. (2006). TTLL7 is a mammalian beta-tubulin polyglutamylase required for growth of MAP2-positive neurites. *J Biol Chem* **281**, 30707-16.

Janke, C. (2014). The tubulin code: Molecular components, readout mechanisms, and functions. *J Cell Biol* **206**, 461-472.

Janke, C., Rogowski, K., Wloga, D., Regnard, C., Kajava, A. V., Strub, J.-M., Temurak, N., van Dijk, J., Boucher, D., van Dorsselaer, A. et al. (2005). Tubulin polyglutamylase enzymes are members of the TTL domain protein family. *Science* **308**, 1758-1762.

Jeong, J.-Y., Yim, H.-S., Ryu, J.-Y., Lee, H. S., Lee, J.-H., Seen, D.-S. and Kang, S. G. (2012). One-step sequence- and ligation-independent cloning as a rapid and versatile cloning method for functional genomics studies. *Appl Environ Microbiol* **78**, 5440-3.

Kaech, S. and Banker, G. (2006). Culturing hippocampal neurons. *Nat Protoc* **1**, 2406-15.

Kalinina, E., Biswas, R., Berezniuk, I., Hermoso, A., Aviles, F. X. and Fricker, L. D. (2007). A novel subfamily of mouse cytosolic carboxypeptidases. *Faseb J* **21**, 836-50.

Karakaya, M., Paketci, C., Altmueller, J., Thiele, H., Hoelker, I., Yis, U. and Wirth, B. (2019). Biallelic variant in AGTPBP1 causes infantile lower motor neuron degeneration and cerebellar atrophy. *Am J Med Genet A* **179**, 1580-1584.

Kim, J.-Y., Woo, S.-Y., Hong, Y. B., Choi, H., Kim, J., Choi, H., Mook-Jung, I., Ha, N., Kyung, J., Koo, S. K. et al. (2016). HDAC6 Inhibitors Rescued the Defective Axonal Mitochondrial Movement in Motor Neurons Derived from the Induced Pluripotent Stem Cells of Peripheral Neuropathy Patients with HSPB1 Mutation. *Stem Cells Int* **2016**, 9475981.

Kim, J. H., Lee, S.-R., Li, L.-H., Park, H.-J., Park, J.-H., Lee, K. Y., Kim, M.-K., Shin, B. A. and Choi, S.-Y. (2011). High cleavage efficiency of a 2A peptide derived from porcine teschovirus-1 in human cell lines, zebrafish and mice. *PLoS ONE* **6**, e18556.

Klinman, E. and Holzbaur, E. L. F. (2016). Comparative analysis of axonal transport markers in primary mammalian neurons. *Methods Cell Biol* **131**, 409-24.

Konishi, Y. and Setou, M. (2009). Tubulin tyrosination navigates the kinesin-1 motor domain to axons. *Nat Neurosci* **12**, 559-67.

Lacroix, B., van Dijk, J., Gold, N. D., Guizetti, J., Aldrian-Herrada, G., Rogowski, K., Gerlich, D. W. and Janke, C. (2010). Tubulin polyglutamylation stimulates spastin-mediated microtubule severing. *J Cell Biol* **189**, 945-54.

Lee, C. W. and Peng, H. B. (2008). The function of mitochondria in presynaptic development at the neuromuscular junction. *Mol Biol Cell* **19**, 150-8.

Lee, S., Sato, Y. and Nixon, R. A. (2011). Lysosomal proteolysis inhibition selectively disrupts axonal transport of degradative organelles and causes an Alzheimer's-like axonal dystrophy. *J Neurosci* **31**, 7817-30.

Lessard, D. V., Zinder, O. J., Hotta, T., Verhey, K. J., Ohi, R. and Berger, C. L. (2019). Polyglutamylation of tubulin's C-terminal tail controls pausing and motility of kinesin-3 family member KIF1A. *J Biol Chem* **294**, 6353-6363.

Lo, K. Y., Kuzmin, A., Unger, S. M., Petersen, J. D. and Silverman, M. A. (2011). KIF1A is the primary anterograde motor protein required for the axonal transport of dense-core vesicles in cultured hippocampal neurons. *Neurosci Lett* **491**, 168-73.

Lu, B., Nagappan, G., Guan, X., Nathan, P. J. and Wren, P. (2013). BDNF-based synaptic repair as a disease-modifying strategy for neurodegenerative diseases. *Nat Rev Neurosci* **14**, 401-16.

Maas, C., Belgardt, D., Lee, H. K., Heisler, F. F., Lappe-Siefke, C., Magiera, M. M., van Dijk, J., Hausrat, T. J., Janke, C. and Kneussel, M. (2009). Synaptic activation modifies microtubules underlying transport of postsynaptic cargo. *Proc Natl Acad Sci U S A* **106**, 8731-6.

Maday, S., Twelvetrees, A. E., Moughamian, A. J. and Holzbaur, E. L. F. (2014). Axonal transport: cargo-specific mechanisms of motility and regulation. *Neuron* **84**, 292-309.

Maday, S., Wallace, K. E. and Holzbaur, E. L. F. (2012). Autophagosomes initiate distally and mature during transport toward the cell soma in primary neurons. *J Cell Biol* **196**, 407-17.

Magiera, M. M., Bodakuntla, S., Ziak, J., Lacomme, S., Marques Sousa, P., Leboucher, S., Hausrat, T. J., Bosc, C., Andrieux, A., Kneussel, M. et al. (2018). Excessive tubulin polyglutamylation causes neurodegeneration and perturbs neuronal transport. *EMBO J* **37**, e100440.

Millecamps, S. and Julien, J.-P. (2013). Axonal transport deficits and neurodegenerative diseases. *Nat Rev Neurosci* **14**, 161-76.

Morris, R. L. and Hollenbeck, P. J. (1993). The regulation of bidirectional mitochondrial transport is coordinated with axonal outgrowth. *J Cell Sci* **104 (Pt 3)**, 917-27.

Moutaux, E., Christaller, W., Scaramuzzino, C., Genoux, A., Charlot, B., Cazorla, M. and Saudou, F. (2018). Neuronal network maturation differently affects secretory vesicles and mitochondria transport in axons. *Sci Rep* **8**, 13429.

Munoz-Castaneda, R., Diaz, D., Peris, L., Andrieux, A., Bosc, C., Munoz-Castaneda, J. M., Janke, C., Alonso, J. R., Moutin, M.-J. and Weruaga, E. (2018). Cytoskeleton stability is essential for the integrity of the cerebellum and its motor- and affective-related behaviors. *Sci Rep* **8**, 3072.

Newton, C. N., DeLuca, J. G., Himes, R. H., Miller, H. P., Jordan, M. A. and Wilson, L. (2002). Intrinsically slow dynamic instability of HeLa cell microtubules in vitro. *J Biol Chem* **277**, 42456-62.

Nieuwenhuis, J., Adamopoulos, A., Bleijerveld, O. B., Mazouzi, A., Stickel, E., Celie, P., Altelaar, M., Knipscheer, P., Perrakis, A., Blomen, V. A. et al. (2017). Vasohibins encode tubulin detyrosinating activity. *Science* **358**, 1453-1456.

Nirschl, J. J., Ghiretti, A. E. and Holzbaur, E. L. F. (2017). The impact of cytoskeletal organization on the local regulation of neuronal transport. *Nat Rev Neurosci* **18**, 585-597.

Pu, J., Guardia, C. M., Keren-Kaplan, T. and Bonifacino, J. S. (2016). Mechanisms and functions of lysosome positioning. *J Cell Sci* **129**, 4329-4339.

Reck-Peterson, S. L., Redwine, W. B., Vale, R. D. and Carter, A. P. (2018). The cytoplasmic dynein transport machinery and its many cargoes. *Nat Rev Mol Cell Biol* **19**, 382-398.

Rogowski, K., van Dijk, J., Magiera, M. M., Bosc, C., Deloulme, J.-C., Bosson, A., Peris, L., Gold, N. D., Lacroix, B., Bosch Grau, M. et al. (2010). A family of protein-deglutamylating enzymes associated with neurodegeneration. *Cell* **143**, 564-578.

Rowland, K. C., Irby, N. K. and Spirou, G. A. (2000). Specialized synapse-associated structures within the calyx of Held. *J Neurosci* **20**, 9135-44.

Rüdiger, M., Plessman, U., Kloppel, K. D., Wehland, J. and Weber, K. (1992). Class II tubulin, the major brain beta tubulin isotype is polyglutamylated on glutamic acid residue 435. *FEBS Lett* **308**, 101-105.

Shahpasand, K., Uemura, I., Saito, T., Asano, T., Hata, K., Shibata, K., Toyoshima, Y., Hasegawa, M. and Hisanaga, S.-I. (2012). Regulation of mitochondrial transport and inter-microtubule spacing by tau phosphorylation at the sites hyperphosphorylated in Alzheimer's disease. *J Neurosci* **32**, 2430-41.

Shashi, V., Magiera, M. M., Klein, D., Zaki, M., Schoch, K., Rudnik-Schoneborn, S., Norman, A., Lopes Abath Neto, O., Dusl, M., Yuan, X. et al. (2018). Loss of tubulin deglutamylase CCP1 causes infantile-onset neurodegeneration. *EMBO J* **37**, e100540.

Sheffer, R., Gur, M., Brooks, R., Salah, S., Daana, M., Fraenkel, N., Eisenstein, E., Rabie, M., Nevo, Y., Jalas, C. et al. (2019). Biallelic variants in AGTPBP1, involved in tubulin deglutamylation, are associated with cerebellar degeneration and motor neuropathy. *Eur J Hum Genet* **27**, 1419-1426.

Shida, T., Cueva, J. G., Xu, Z., Goodman, M. B. and Nachury, M. V. (2010). The major alpha-tubulin K40 acetyltransferase alphaTAT1 promotes rapid ciliogenesis and efficient mechanosensation. *Proc Natl Acad Sci U S A* **107**, 21517-21522.

Sirajuddin, M., Rice, L. M. and Vale, R. D. (2014). Regulation of microtubule motors by tubulin isotypes and post-translational modifications. *Nat Cell Biol* **16**, 335-44.

Sleigh, J. N., Rossor, A. M., Fellows, A. D., Tosolini, A. P. and Schiavo, G. (2019). Axonal transport and neurological disease. *Nat Rev Neurol*, 10.1038/s41582-019-0257-2.

Stephan, R., Goellner, B., Moreno, E., Frank, C. A., Hugenschmidt, T., Genoud, C., Aberle, H. and Pielage, J. (2015). Hierarchical microtubule organization controls axon caliber and transport and determines synaptic structure and stability. *Dev Cell* **33**, 5-21.

Sullivan, K. F. and Cleveland, D. W. (1986). Identification of conserved isotype-defining variable region sequences for four vertebrate beta tubulin polypeptide classes. *Proc Natl Acad Sci U S A* **83**, 4327-31.

Tas, R. P., Chazeau, A., Cloin, B. M. C., Lambers, M. L. A., Hoogenraad, C. C. and Kapitein, L. C. (2017). Differentiation between Oppositely Oriented Microtubules Controls Polarized Neuronal Transport. *Neuron* **96**, 1264-1271 e5.

Tort, O., Tanco, S., Rocha, C., Bieche, I., Seixas, C., Bosc, C., Andrieux, A., Moutin, M.-J., Xavier Aviles, F., Lorenzo, J. et al. (2014). The cytosolic carboxypeptidases CCP2 and CCP3 catalyze posttranslational removal of acidic amino acids. *Mol Biol Cell* **25**, 3017-3027.

Tortosa, E., Kapitein, L. C. and Hoogenraad, C. C. (2016). Microtubule Organization and Microtubule-Associated Proteins (MAPs). In *Dendrites: Development and Disease*, (eds K. Emoto R. Wong E. Huang and C. Hoogenraad), pp. 31-75: Springer Japan.

Valenstein, M. L. and Roll-Mecak, A. (2016). Graded Control of Microtubule Severing by Tubulin Glutamylation. *Cell* **164**, 911-21.

van Dijk, J., Rogowski, K., Miro, J., Lacroix, B., Eddé, B. and Janke, C. (2007). A targeted multienzyme mechanism for selective microtubule polyglutamylation. *Mol Cell* **26**, 437-48.

Velez, J. I., Lopera, F., Patel, H. R., Johar, A. S., Cai, Y., Rivera, D., Tobon, C., Villegas, A., Sepulveda-Falla, D., Lehmann, S. G. et al. (2016). Mutations modifying sporadic Alzheimer's disease age of onset. *Am J Med Genet B Neuropsychiatr Genet* **171**, 1116-1130.

Vershinin, M., Carter, B. C., Razafsky, D. S., King, S. J. and Gross, S. P. (2007). Multiple-motor based transport and its regulation by Tau. *Proc Natl Acad Sci U S A* **104**, 87-92.

Virlogeux, A., Moutaux, E., Christaller, W., Genoux, A., Bruyere, J., Fino, E., Charlot, B., Cazorla, M. and Saudou, F. (2018). Reconstituting Corticostriatal Network on-a-Chip Reveals the Contribution of the Presynaptic Compartment to Huntington's Disease. *Cell Rep* **22**, 110-122.

Yogev, S., Cooper, R., Fetter, R., Horowitz, M. and Shen, K. (2016). Microtubule Organization Determines Axonal Transport Dynamics. *Neuron* **92**, 449-460.

Zala, D., Hinckelmann, M.-V., Yu, H., Lyra da Cunha, M. M., Liot, G., Cordelieres, F. P., Marco, S. and Saudou, F. (2013). Vesicular glycolysis provides on-board energy for fast axonal transport. *Cell* **152**, 479-91.

Zeng, H. and Sanes, J. R. (2017). Neuronal cell-type classification: challenges, opportunities and the path forward. *Nat Rev Neurosci* **18**, 530-546.

Zhou, B., Yu, P., Lin, M.-Y., Sun, T., Chen, Y. and Sheng, Z.-H. (2016). Facilitation of axon regeneration by enhancing mitochondrial transport and rescuing energy deficits. *J Cell Biol* **214**, 103-19.

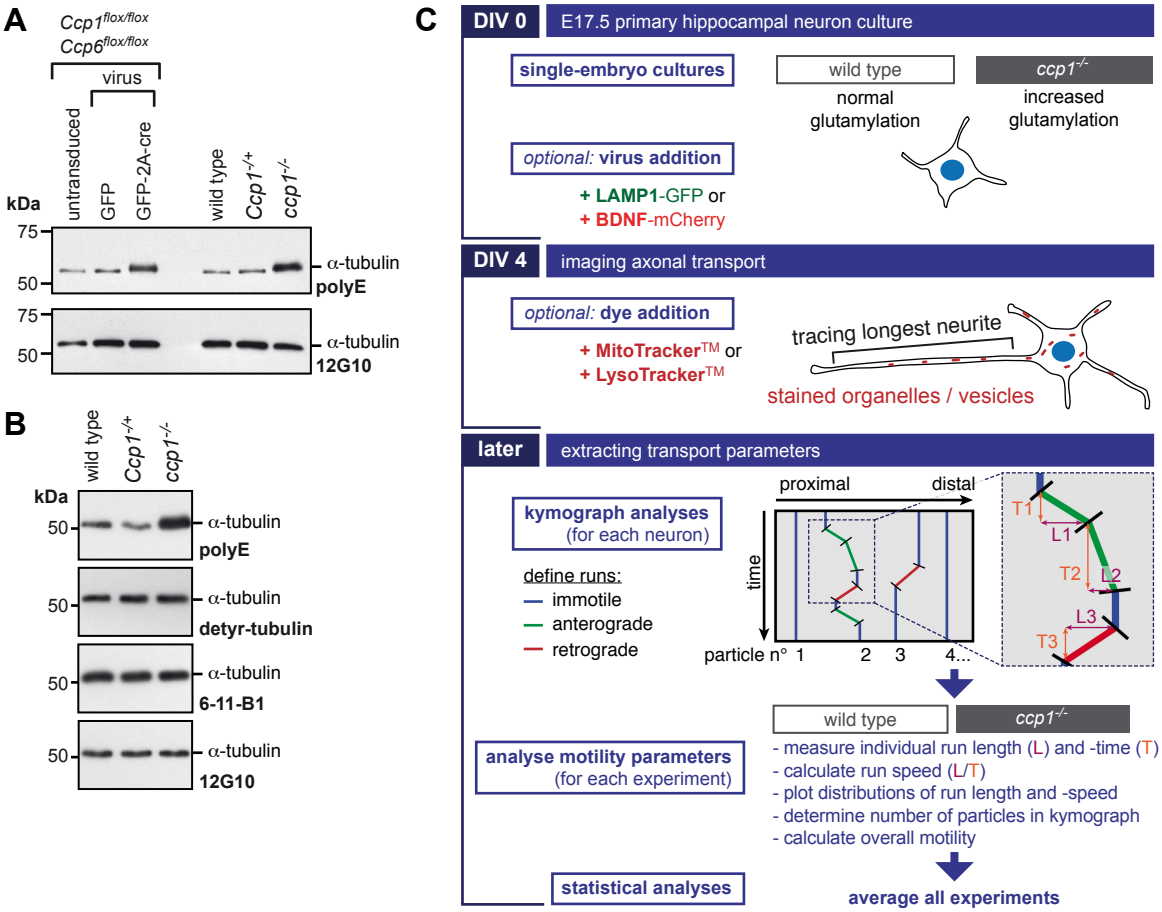
A
Ccp1flox/flox
Ccp6flox/flox
virus
untransduced
GFP
GFP-2A-cre
wild type
Ccp1-/+
ccp1-/-
kDa
75
50
α-tubulin
polyE
α-tubulin
12G10
B
wild type
Ccp1-/+
ccp1-/-
kDa
50
α-tubulin
polyE
α-tubulin
detyr-tubulin
α-tubulin
6-11-B1
α-tubulin
12G10
C
DIV 0
E17.5 primary hippocampal neuron culture
single-embryo cultures
wild type
normal glutamylation
ccp1-/-
increased glutamylation
optional: virus addition
+ LAMP1-GFP or
+ BDNF-mCherry
DIV 4
imaging axonal transport
optional: dye addition
+ MitoTracker™ or
+ LysoTracker™
tracing longest neurite
stained organelles / vesicles
later
extracting transport parameters
kymograph analyses
(for each neuron)
define runs:
immotile
anterograde
retrograde
proximal
distal
time
particle n° 1
2
3
4...
T1
L1
T2
L2
L3
T3
wild type
ccp1-/-
analyse motility parameters
(for each experiment)
- measure individual run length (L) and -time (T)
- calculate run speed (L/T)
- plot distributions of run length and -speed
- determine number of particles in kymograph
- calculate overall motility
statistical analyses
average all experiments

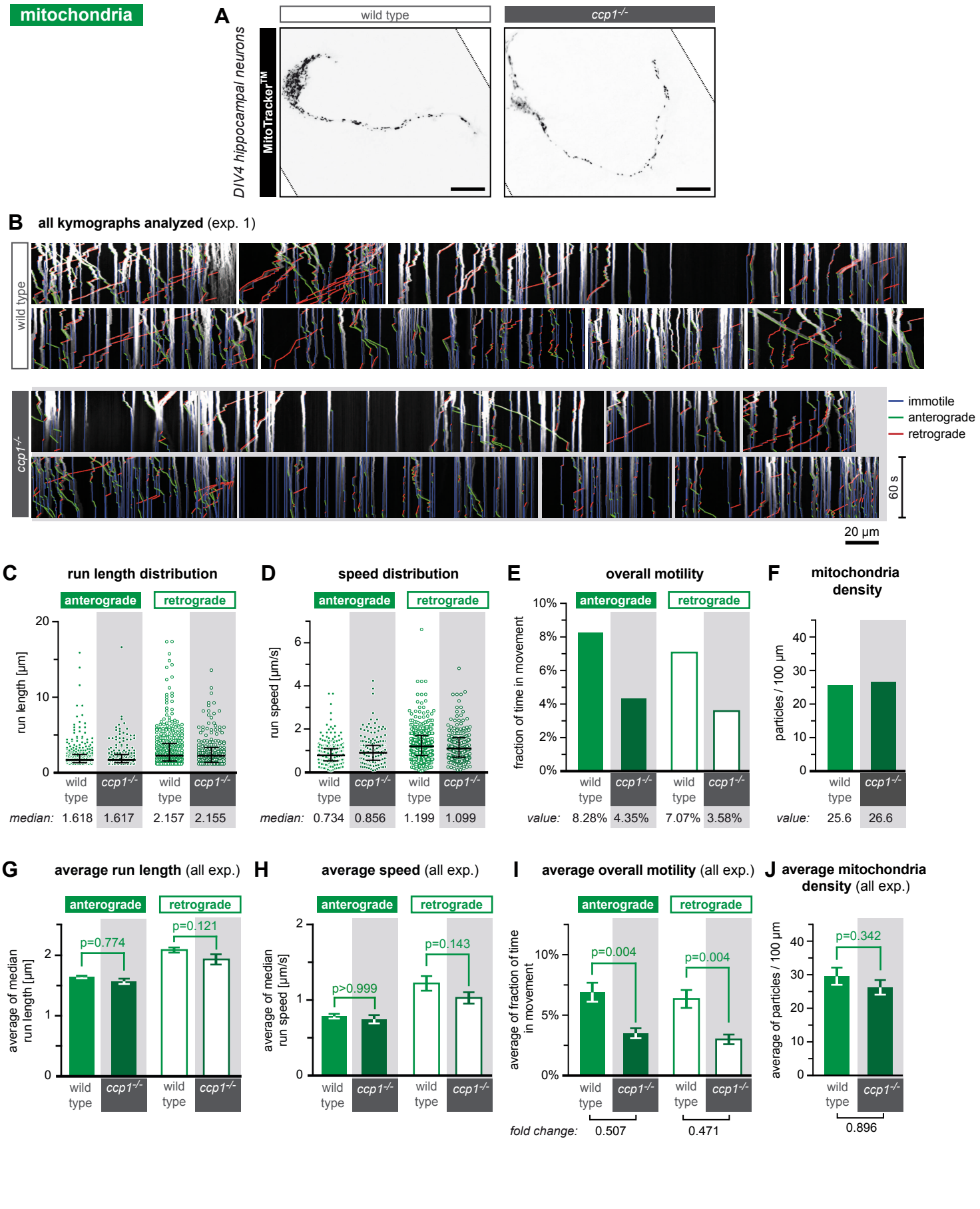
mitochondria
A
wild type
ccp1-/-
DIV4 hippocampal neurons
MitoTracker™
B all kymographs analyzed (exp. 1)
wild type
ccp1-/-
immotile
anterograde
retrograde
60 s
20 µm
C run length distribution
anterograde
retrograde
run length [µm]
wild type
ccp1-/-
median: 1.618 1.617 2.157 2.155
D speed distribution
run speed [µm/s]
median: 0.734 0.856 1.199 1.099
E overall motility
fraction of time in movement
value: 8.28% 4.35% 7.07% 3.58%
F mitochondria density
particles / 100 µm
value: 25.6 26.6
G average run length (all exp.)
average of median run length [µm]
p=0.774
p=0.121
H average speed (all exp.)
average of median run speed [µm/s]
p>0.999
p=0.143
I average overall motility (all exp.)
average of fraction of time in movement
p=0.004
p=0.004
fold change: 0.507 0.471
J average mitochondria density (all exp.)
average of particles / 100 µm
p=0.342
0.896

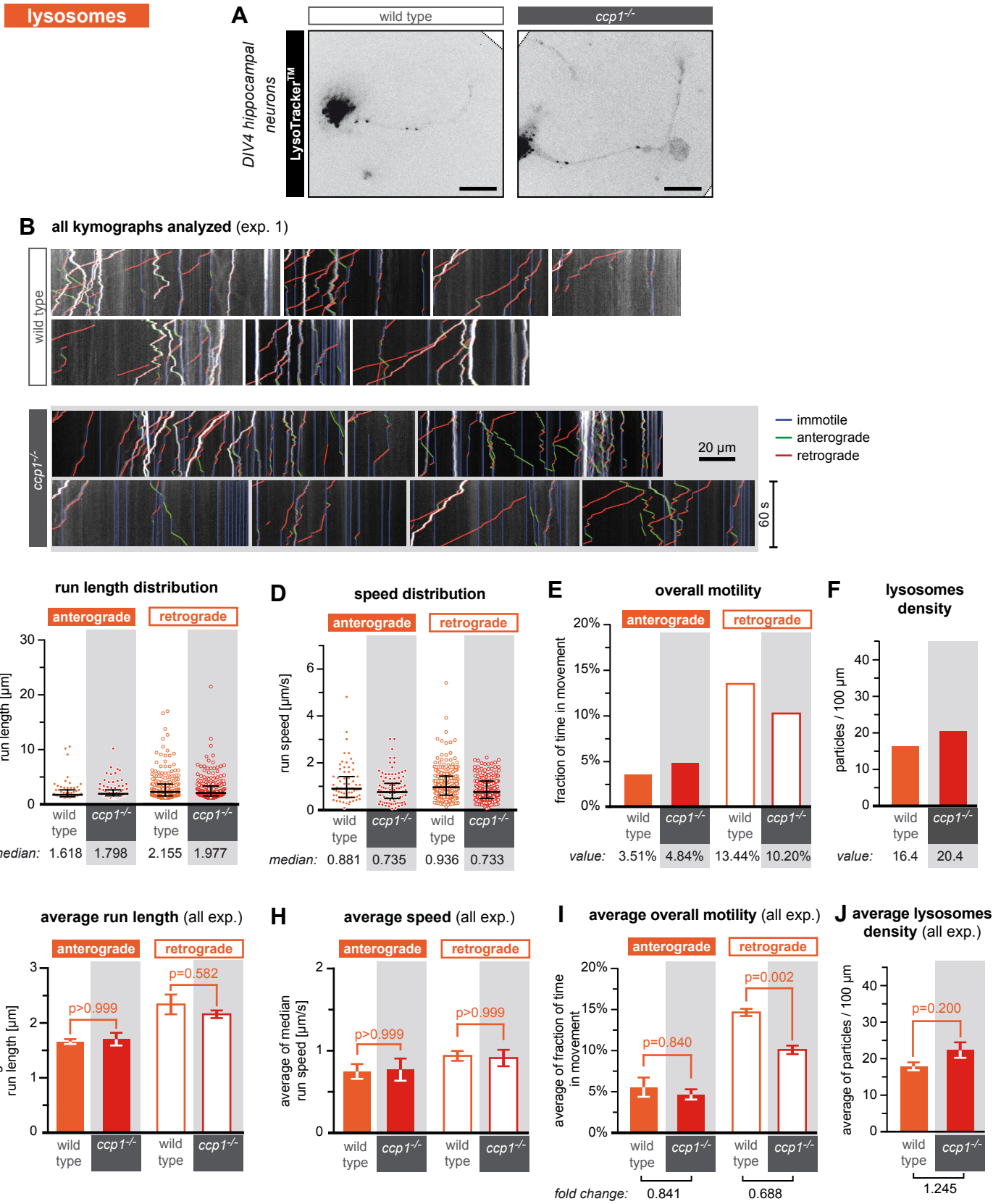
lysosomes
A
wild type
ccp1-/-
DIV4 hippocampal neurons
LysoTracker™
B
all kymographs analyzed (exp. 1)
wild type
ccp1-/-
20 µm
60 s
immotile
anterograde
retrograde
C
run length distribution
anterograde
retrograde
run length [µm]
wild type
ccp1-/-
median: 1.618 1.798 2.155 1.977
D
speed distribution
run speed [µm/s]
median: 0.881 0.735 0.936 0.733
E
overall motility
fraction of time in movement
value: 3.51% 4.84% 13.44% 10.20%
F
lysosomes density
particles / 100 µm
value: 16.4 20.4
G
average run length (all exp.)
average of median run length [µm]
p>0.999
p=0.582
H
average speed (all exp.)
average of median run speed [µm/s]
p>0.999
p>0.999
I
average overall motility (all exp.)
average of fraction of time in movement
p=0.840
p=0.002
fold change: 0.841 0.688
J
average lysosomes density (all exp.)
average of particles / 100 µm
p=0.200
1.245

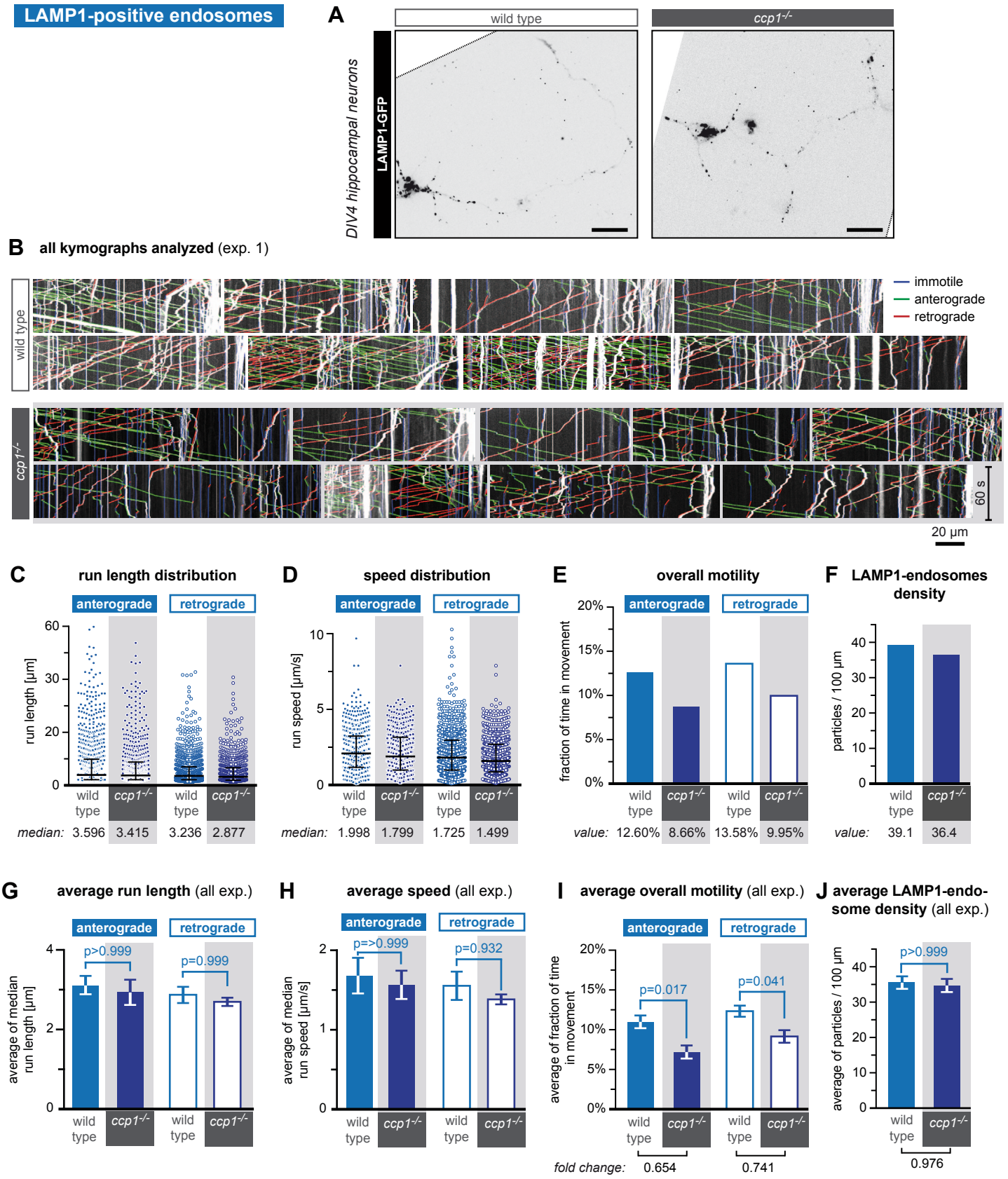
LAMP1-positive endosomes
A
wild type
ccp1-/-
DIV4 hippocampal neurons
LAMP1-GFP
B all kymographs analyzed (exp. 1)
wild type
ccp1-/-
immotile
anterograde
retrograde
60 s
20 µm
C run length distribution
anterograde
retrograde
run length [µm]
median: 3.596 3.415 3.236 2.877
D speed distribution
run speed [µm/s]
median: 1.998 1.799 1.725 1.499
E overall motility
fraction of time in movement
value: 12.60% 8.66% 13.58% 9.95%
F LAMP1-endosomes density
particles / 100 µm
value: 39.1 36.4
G average run length (all exp.)
average of median run length [µm]
p>0.999
p=0.999
H average speed (all exp.)
average of median run speed [µm/s]
p=>0.999
p=0.932
I average overall motility (all exp.)
average of fraction of time in movement
p=0.017
p=0.041
fold change: 0.654 0.741
J average LAMP1-endosome density (all exp.)
average of particles / 100 µm
p>0.999
0.976

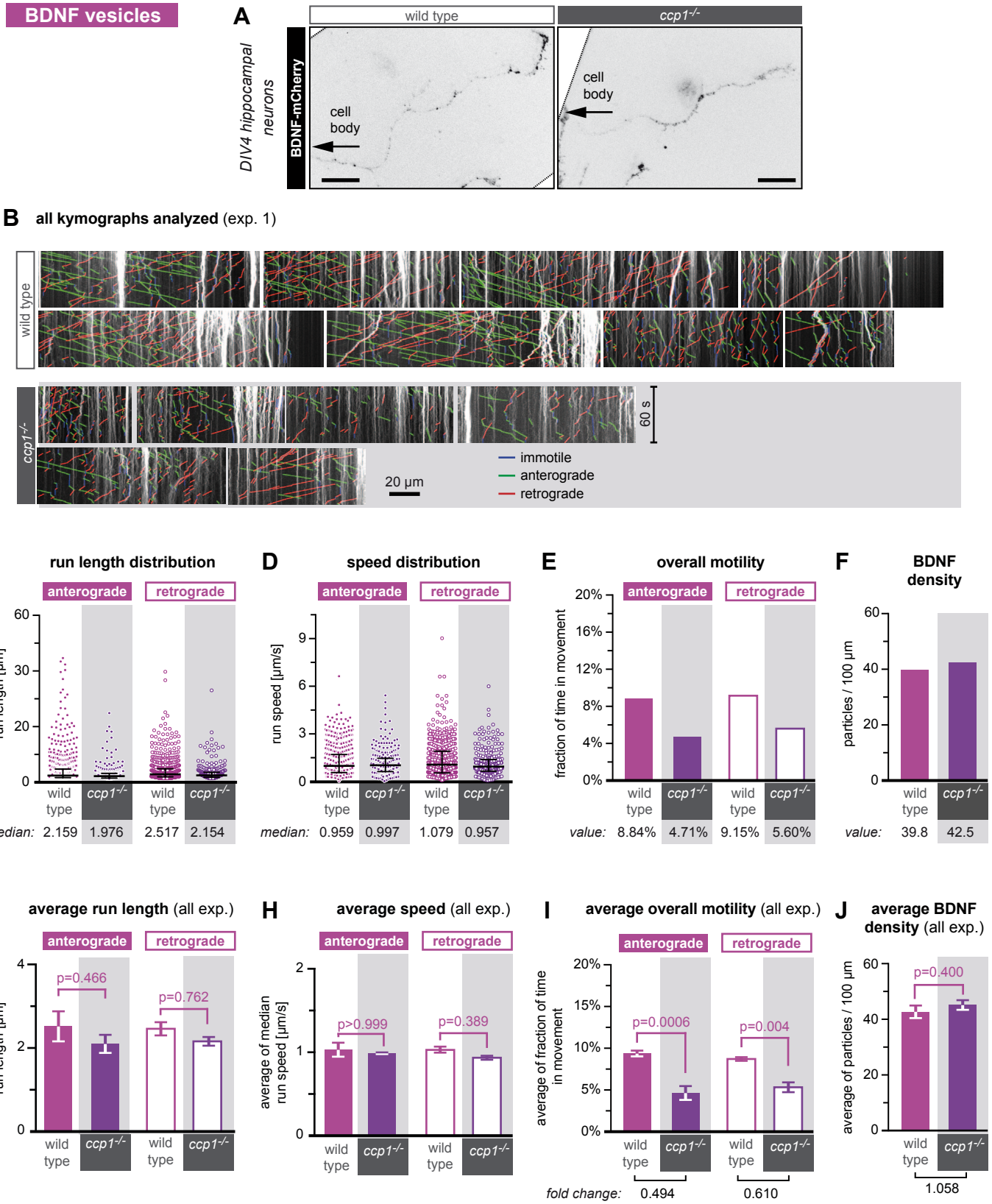
BDNF vesicles
A
wild type
ccp1-/-
DIV4 hippocampal neurons
BDNF-mCherry
cell body
cell body
B all kymographs analyzed (exp. 1)
wild type
ccp1-/-
60 s
20 µm
immotile
anterograde
retrograde
C run length distribution
anterograde
retrograde
run length [µm]
median: 2.159 1.976 2.517 2.154
D speed distribution
run speed [µm/s]
median: 0.959 0.997 1.079 0.957
E overall motility
fraction of time in movement
value: 8.84% 4.71% 9.15% 5.60%
F BDNF density
particles / 100 µm
value: 39.8 42.5
G average run length (all exp.)
average of median run length [µm]
p=0.466
p=0.762
H average speed (all exp.)
average of median run speed [µm/s]
p>0.999
p=0.389
I average overall motility (all exp.)
average of fraction of time in movement
p=0.0006
p=0.004
fold change: 0.494 0.610
J average BDNF density (all exp.)
average of particles / 100 µm
p=0.400
1.058

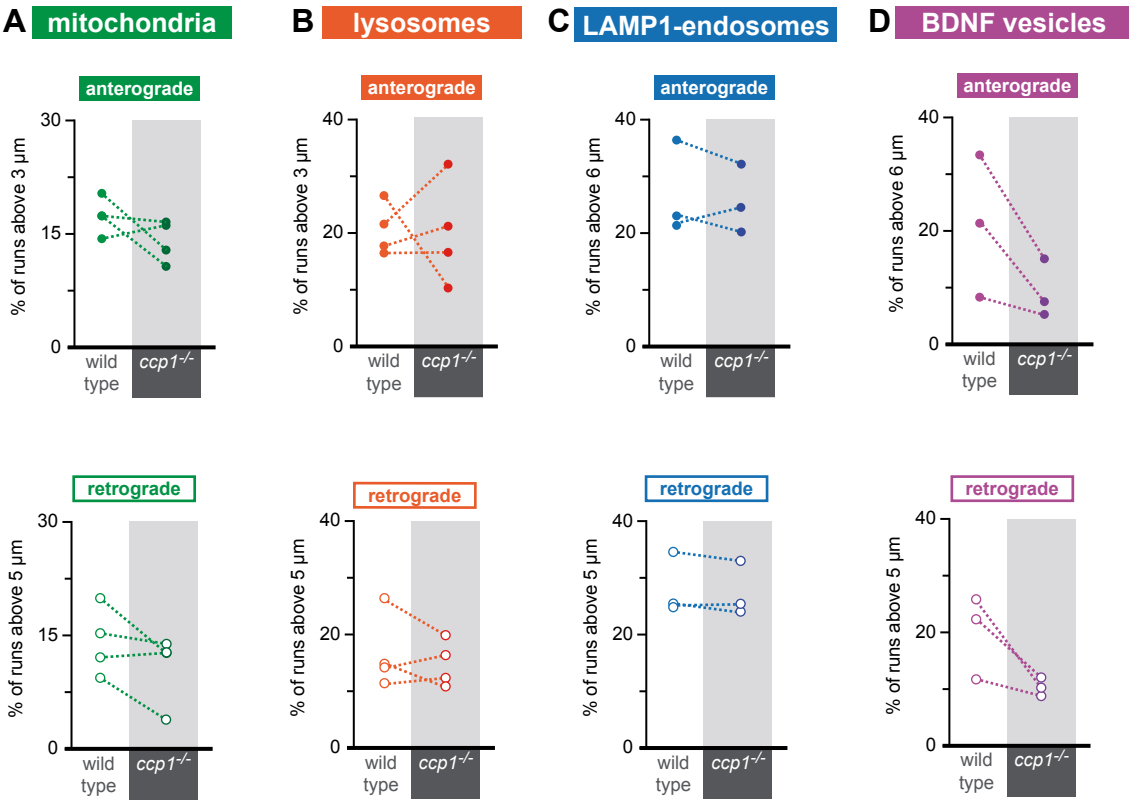
A mitochondria
B lysosomes
C LAMP1-endosomes
D BDNF vesicles
anterograde
retrograde
% of runs above 3 µm
% of runs above 5 µm
% of runs above 6 µm
wild type
ccp1-/-

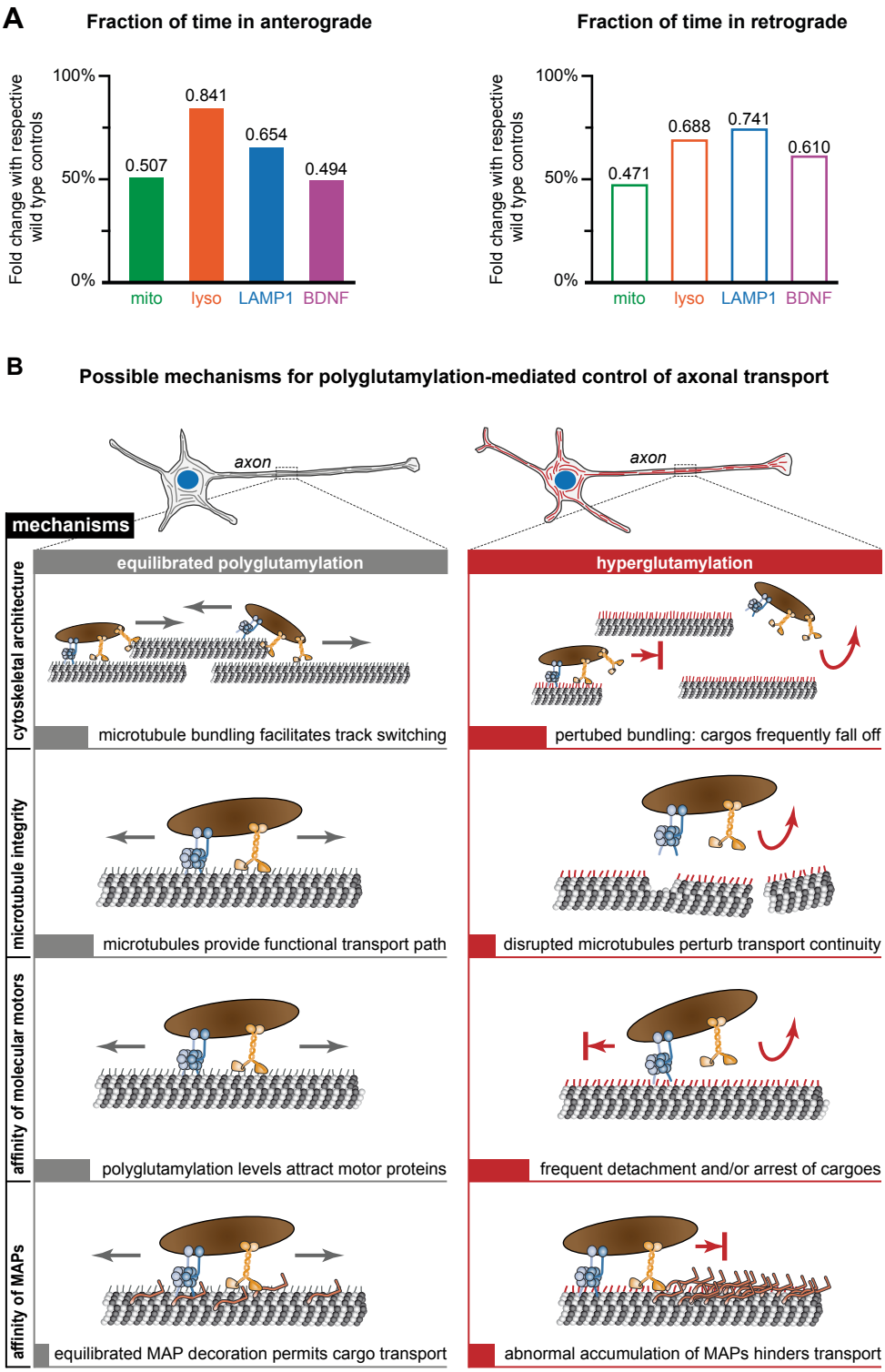
A
Fraction of time in anterograde
Fraction of time in retrograde
Fold change with respective wild type controls
100%
50%
0%
0.507
0.841
0.654
0.494
0.471
0.688
0.741
0.610
mito
lyso
LAMP1
BDNF
B
Possible mechanisms for polyglutamylation-mediated control of axonal transport
axon
mechanisms
equilibrated polyglutamylation
hyperglutamylation
cytoskeletal architecture
microtubule bundling facilitates track switching
pertubed bundling: cargos frequently fall off
microtubule integrity
microtubules provide functional transport path
disrupted microtubules perturb transport continuity
affinity of molecular motors
polyglutamylation levels attract motor proteins
frequent detachment and/or arrest of cargoes
affinity of MAPs
equilibrated MAP decoration permits cargo transport
abnormal accumulation of MAPs hinders transport